伺服馬達之驅動與智慧型控制
Intelligent Control of Servo Motor Drives

國立中央大學電機工程學系講座教授
林法正
E-mail: linfj@ee.ncu.edu.tw

Sep. 23, 2016

Applications of Power Converters

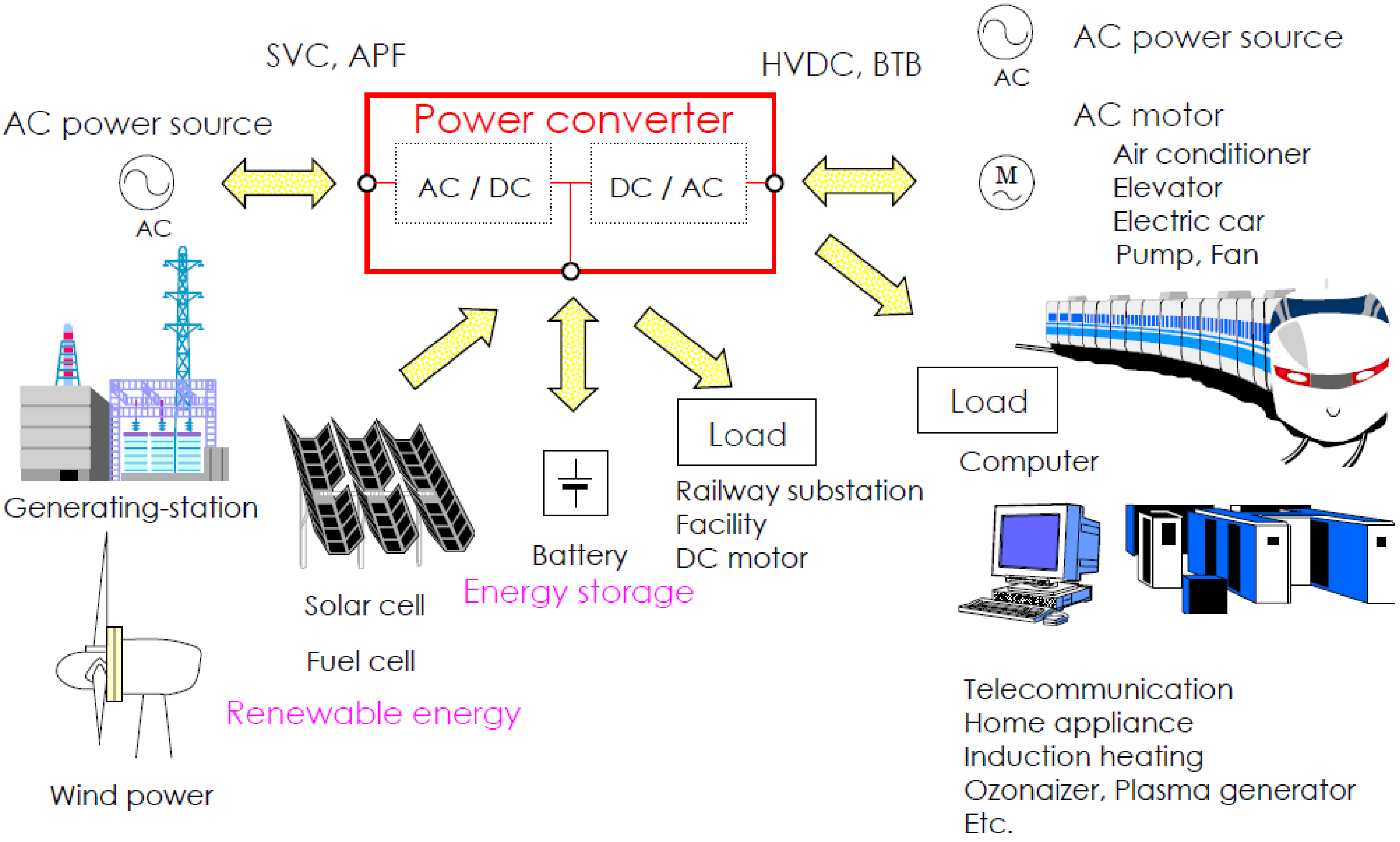

Classification of Power Converter Applications

	Low Power	Medium Power	High Power
Power range	Up to 2 kW	2 kW – 500 kW	More than 500 kW
Usual converter topologies	AC/DC, DC/DC	AC/DC, DC/DC, DC/AC	AC/DC, DC/AC
Typical power semiconductors	MOSFET	MOSFET, IGBT	IGBT, IGCT, THYRISTOR
Technology trend	High power density High efficiency	Small volume and weight Low cost and high efficiency	High nominal power of the converter High power quality and stability
Typical applications	 Low power devices  Appliances	 Electric Vehicles  Roof PV	 Renewable Energy  Transportation  Power Distribution  Industry

馬達驅動器

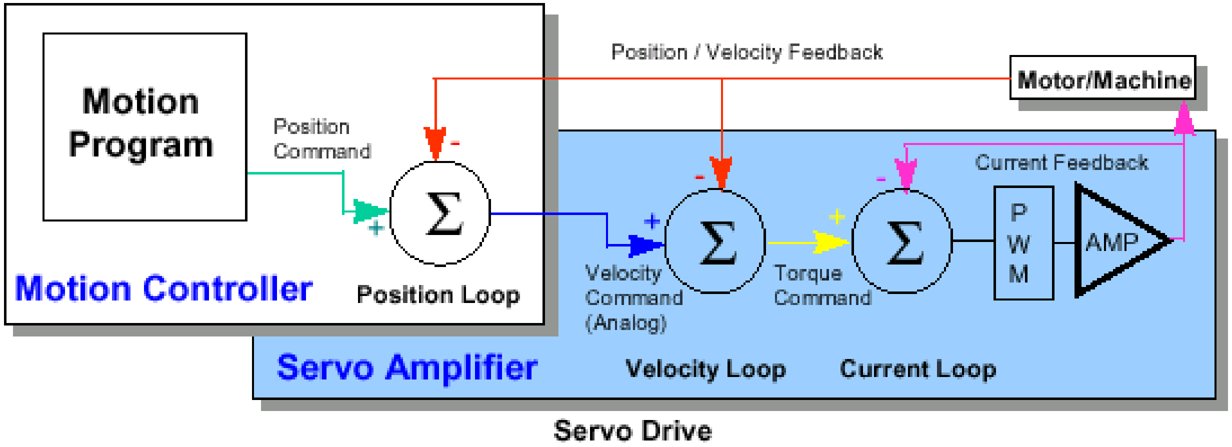

Analog Servo Structure

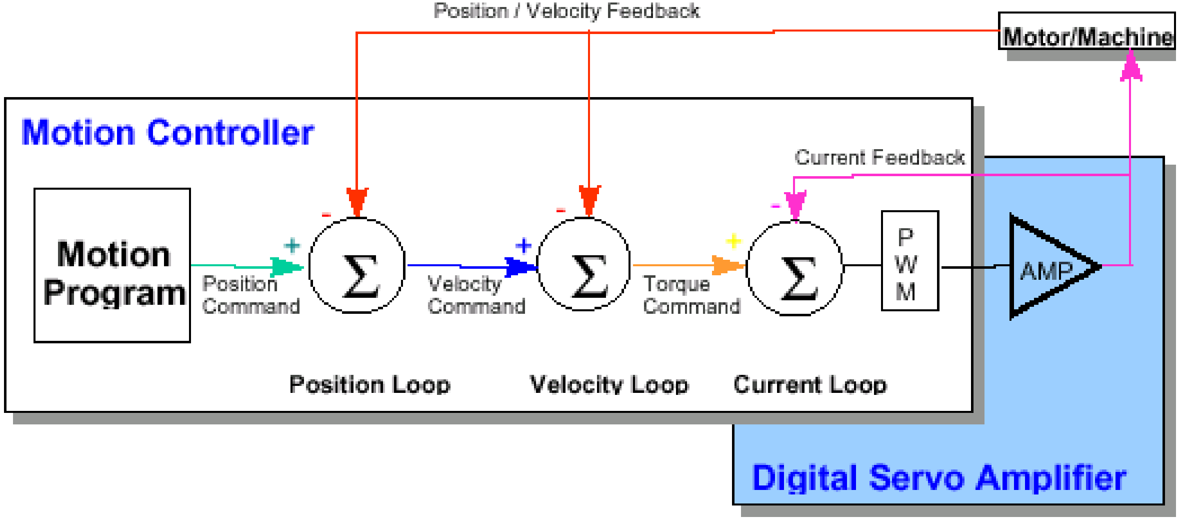

Digital Servo Structure

運動控制器

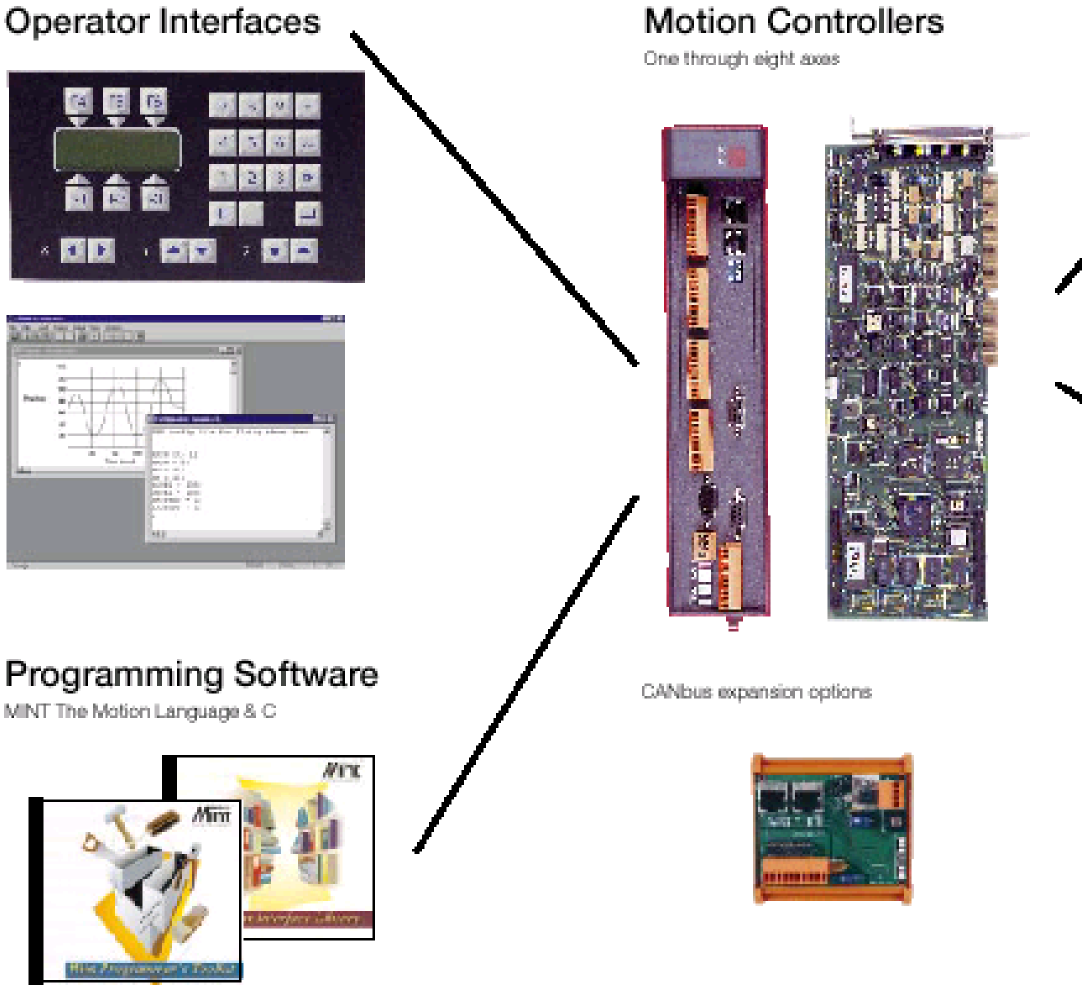

Operator Interfaces

Programming Software

MINT The Motion Language & C

Motion Controllers

One through eight axes

CANbus expansion options

系統應用

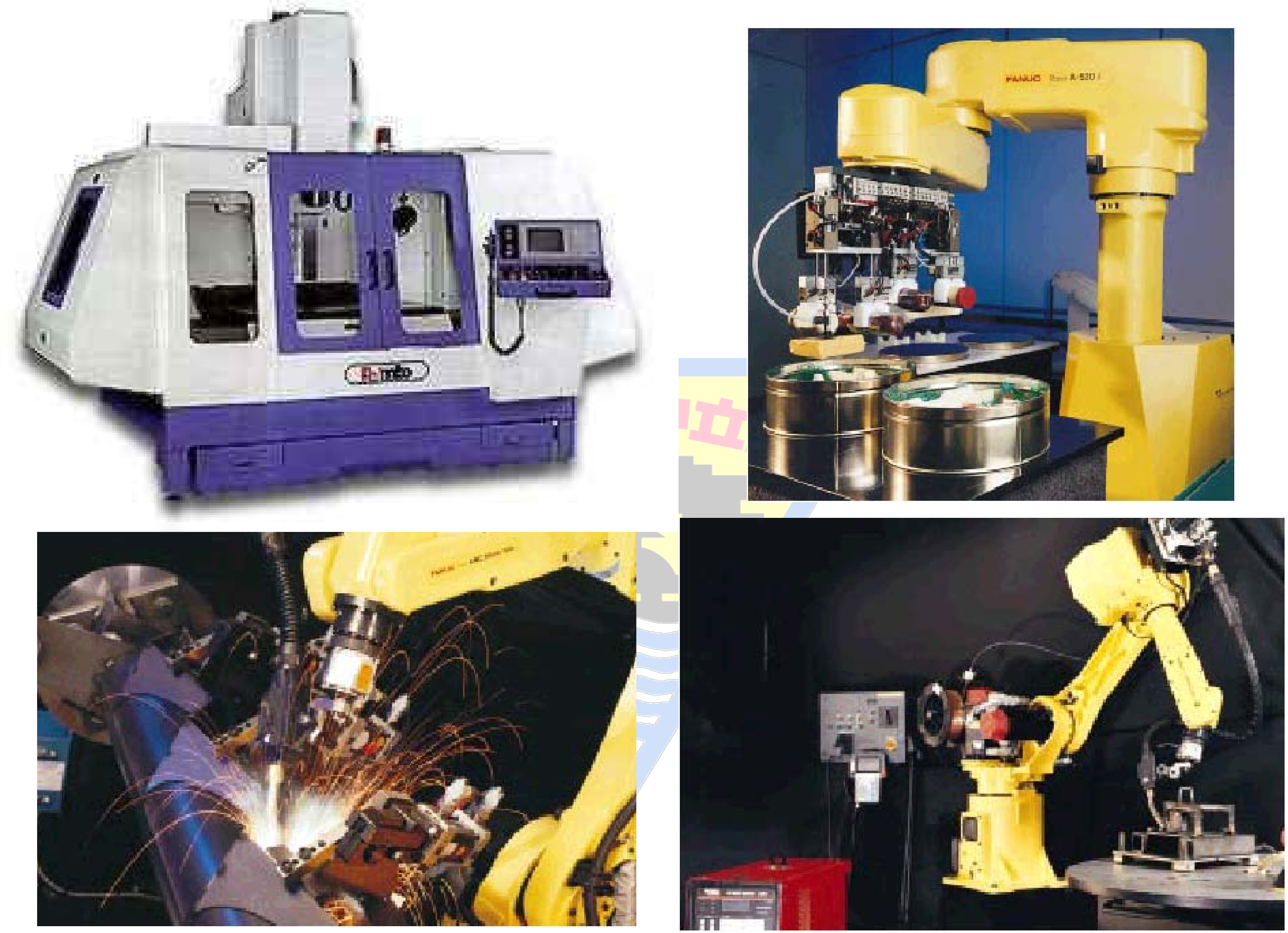

Products of various kinds of EVs


Smart EV


Mitsubishi iMiEV


Nissan LEAF


Luxgen EV+


Honda Fit EV


Mini E


Chevrolet Spark EV


Ford Focus Electric

EV


Toyota Prius


Toyota Camry Hybrid


Lexus GS450h


Honda Civic Hybrid


Porsche Cayenne S Hybrid

HEV


Porsche Panamera
S E Hybrid


Volvo XC60
Plug-In Hybrid


Mitsubishi Outlander PHEV


Toyota Prius Plug-In


Chevrolet Volt


Honda Accord Plug-In


Cadillac ELR

PHEV

Applications of PMSM Servo Drives

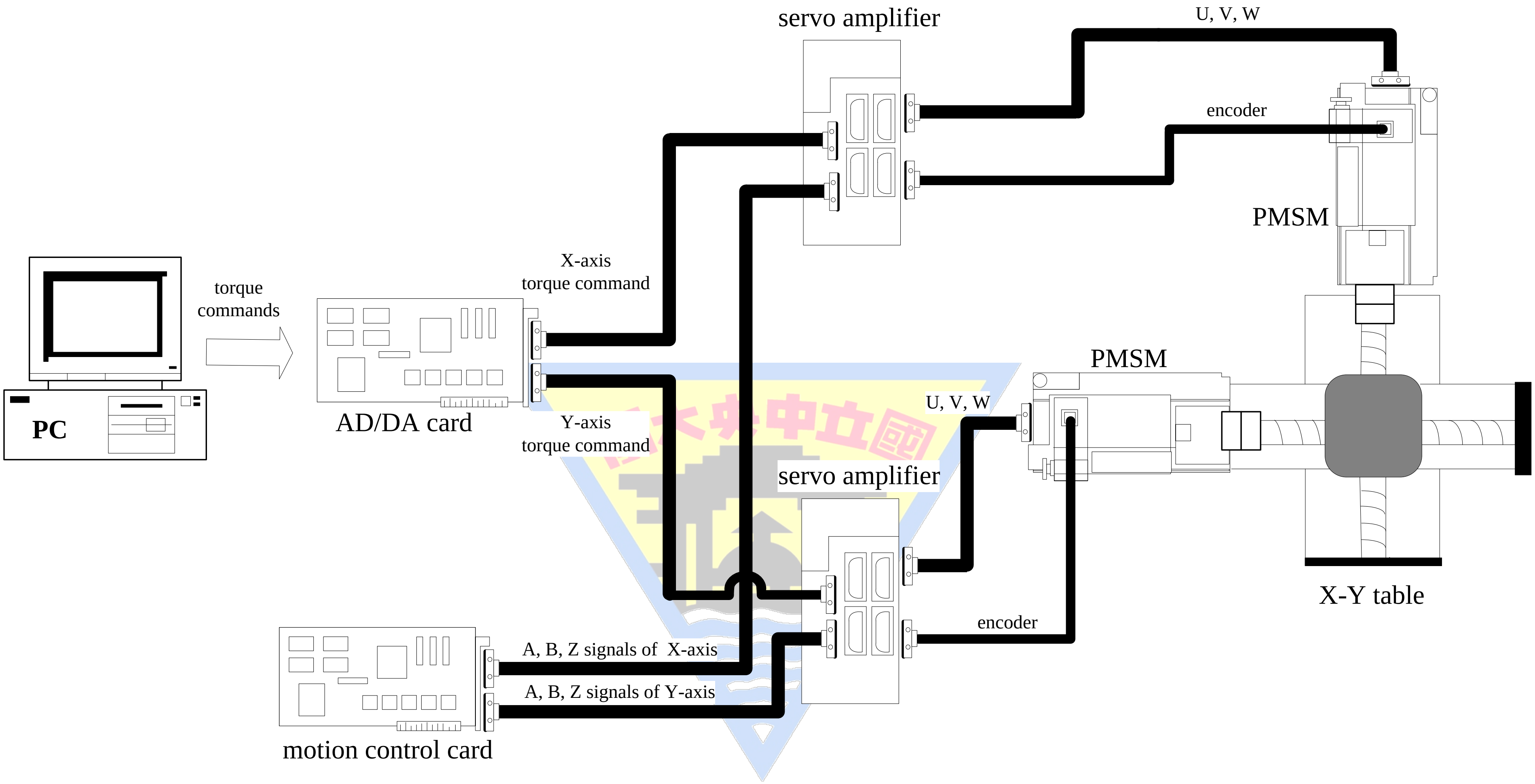

Fig. 1 X-Y table using PMSM in CNC machine

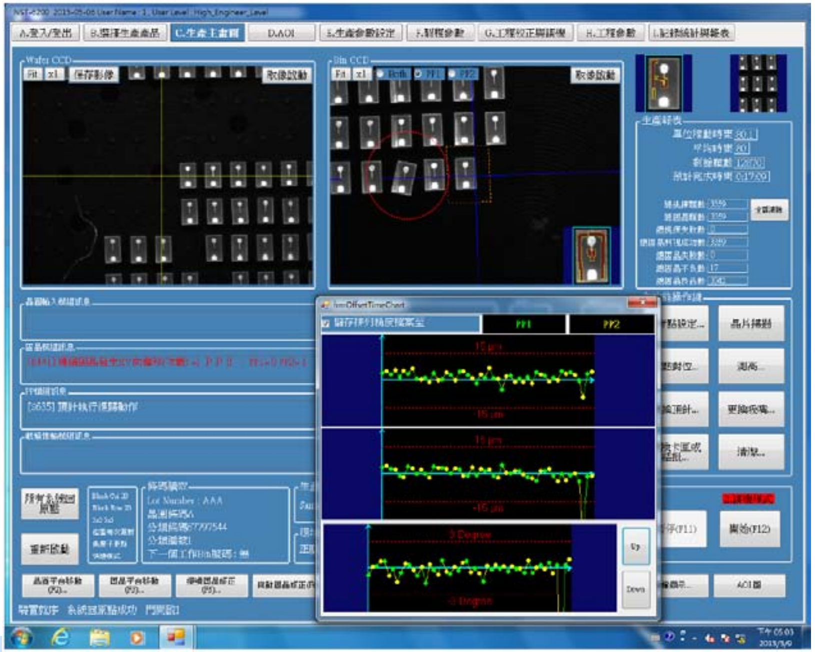

圖3 晶粒排列不良的結果圖

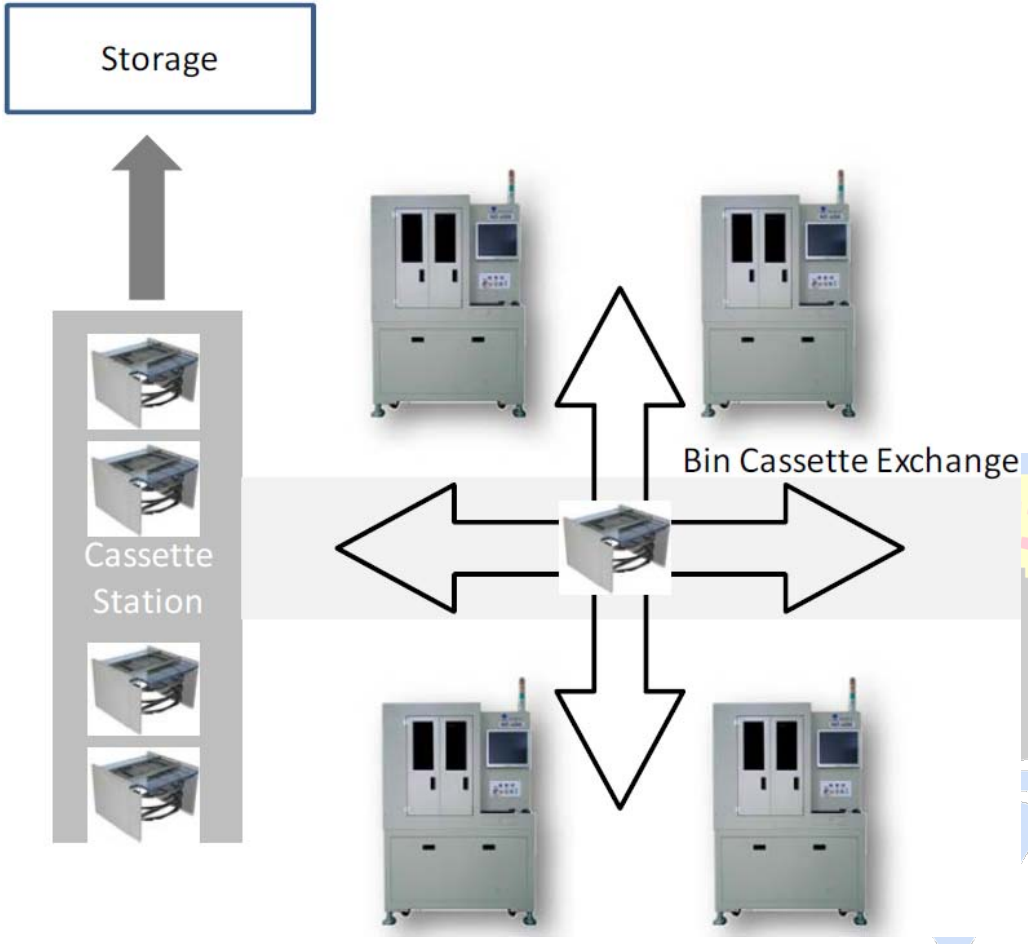

圖2 全自動LED Side Bin Sorter and Cassette Station

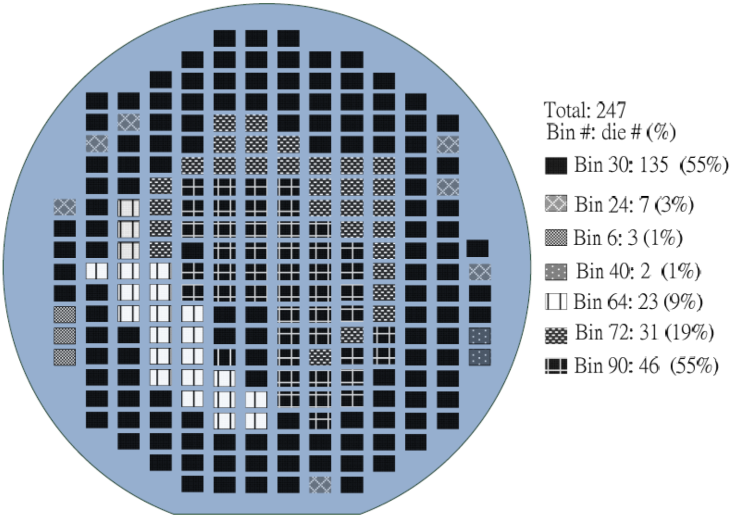

圖4 LED 晶圓之晶粒等級示意圖(藍膜)

Applications Linear Motor Drives

- **Linear Synchronous Motor Drives (3 phase)**
  - Packaging and Material Handling
  - Automated Assembly
  - Reciprocating compressors and alternators
- **Large Linear Induction Motor Drives (3 phase)**
  - Transportation
  - Materials handling
  - Extrusion presses

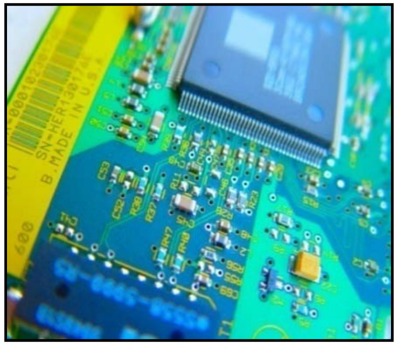

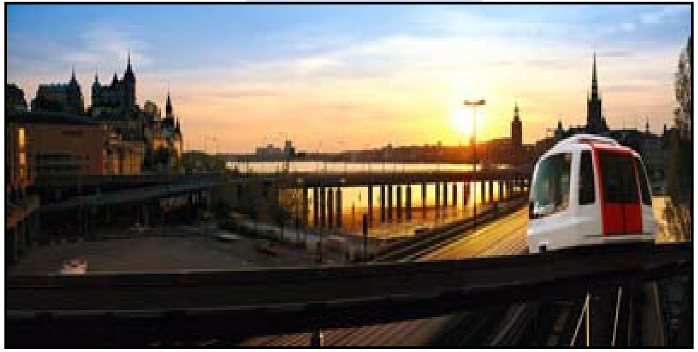

Applications of Fuzzy Logic Systems

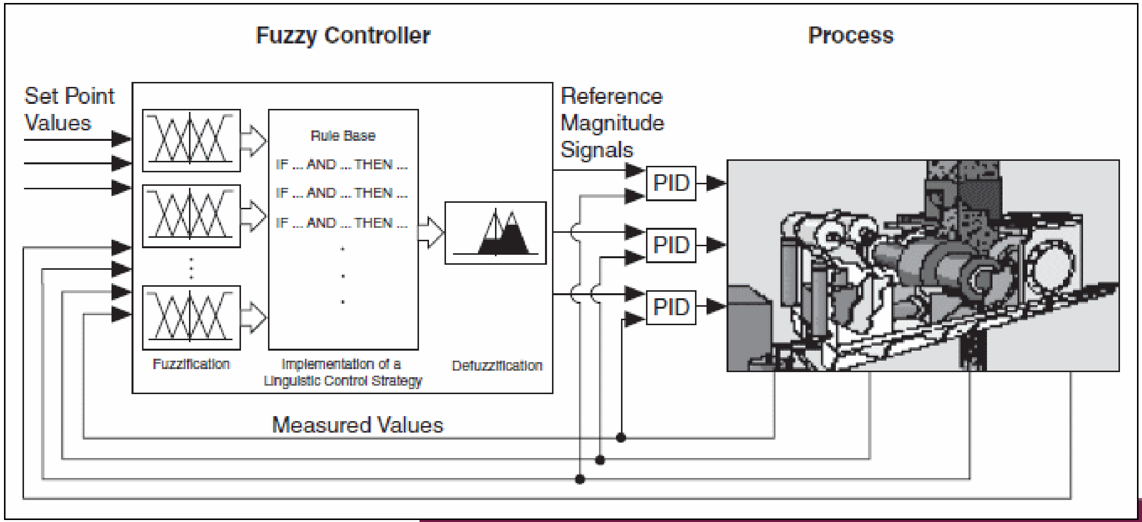

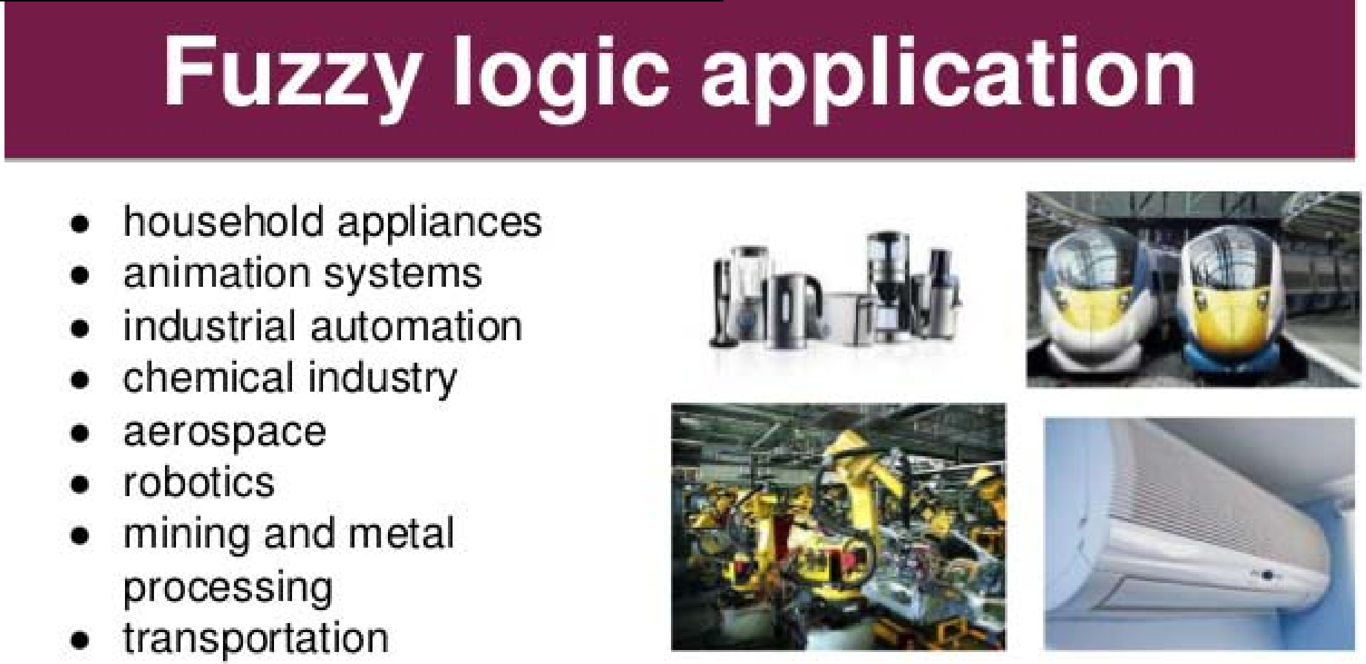

Fuzzy logic application

- household appliances
- animation systems
- industrial automation
- chemical industry
- aerospace
- robotics
- mining and metal processing
- transportation

Applications of Neural Network: Alphago

New search algorithm that combines Monte-Carlo simulation with value and policy networks

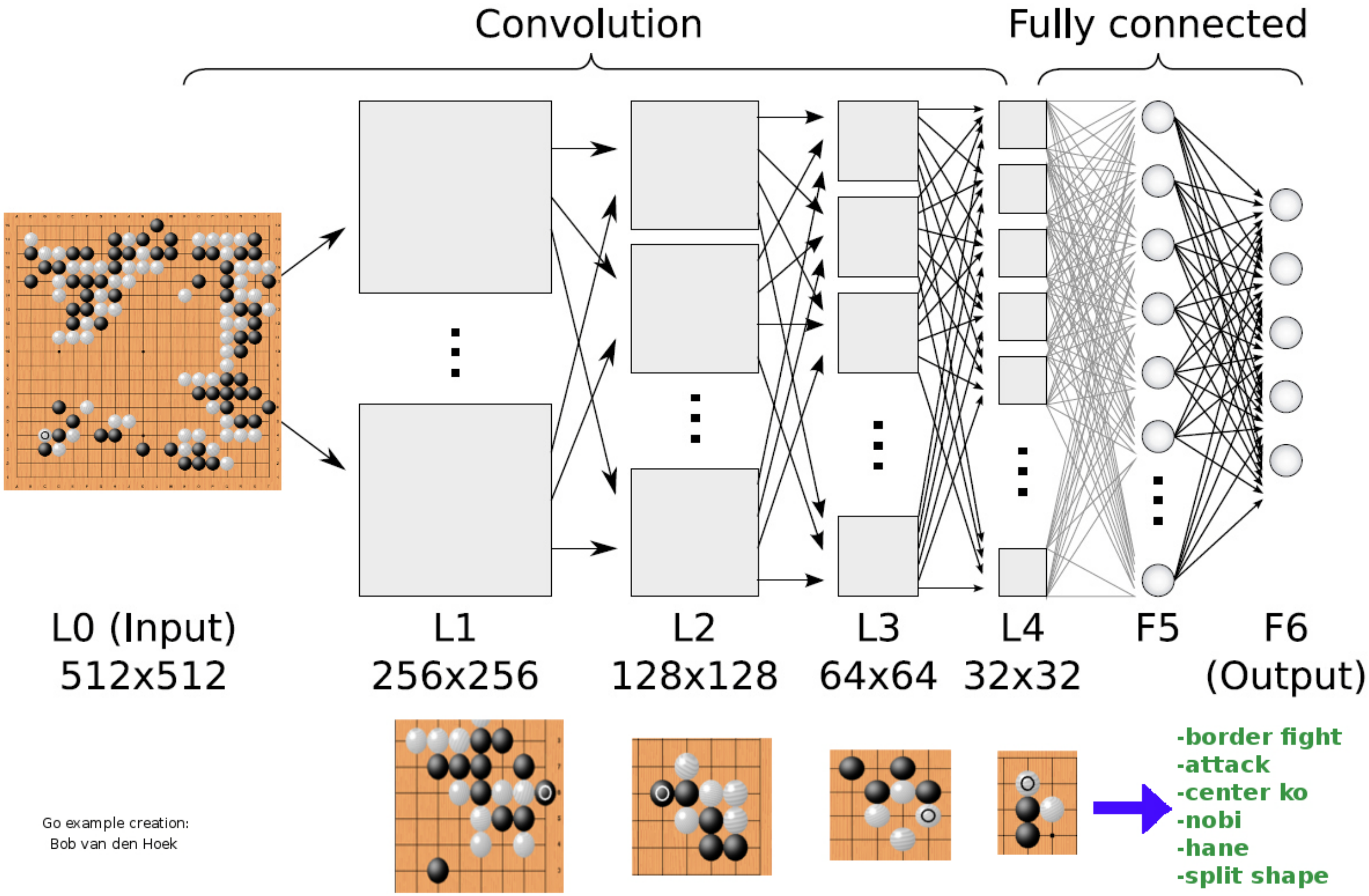

Go example creation:
Bob van den Hoek

Linear Synchronous Motor Drive

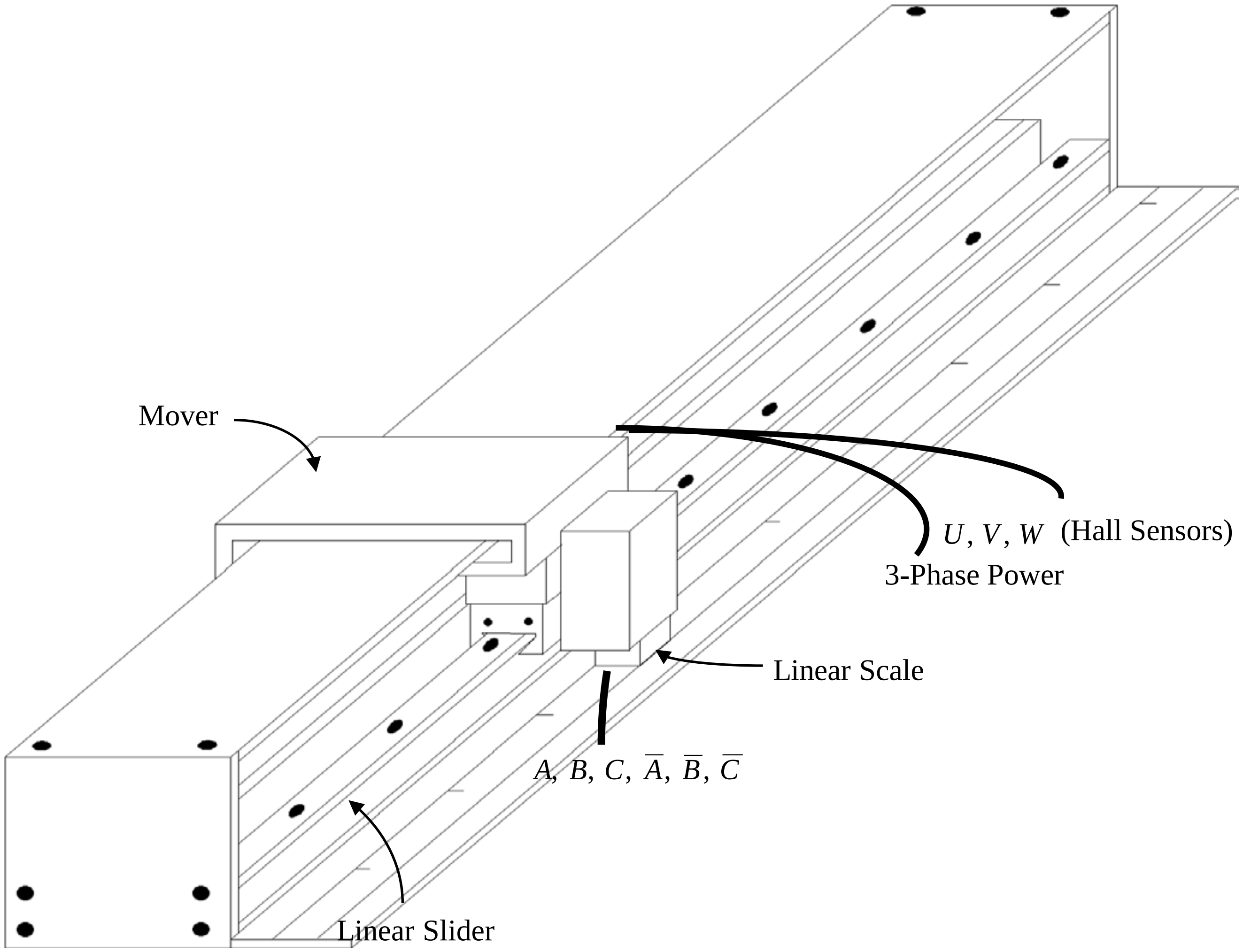

Fig. 5

Linear Synchronous Motor Drive

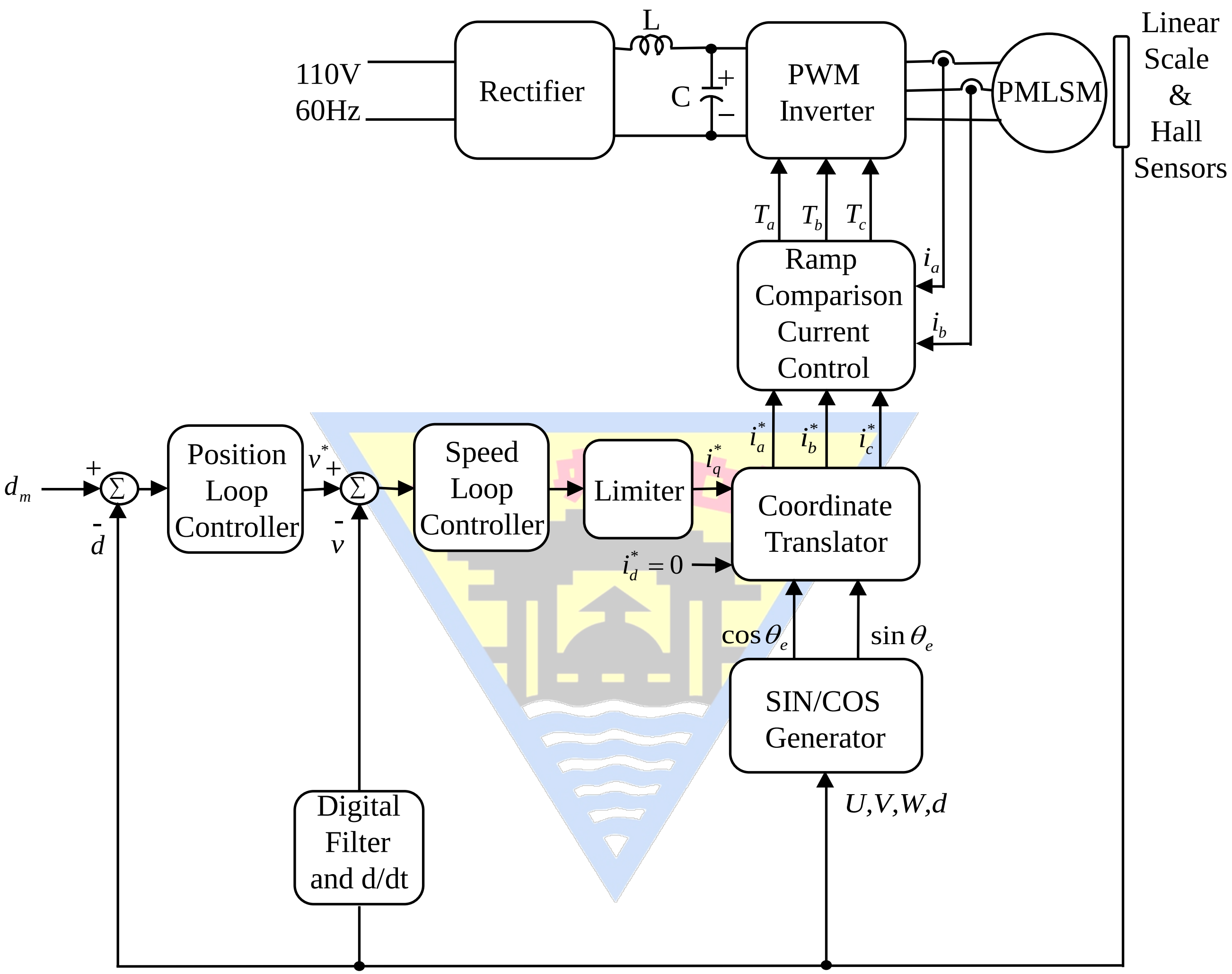

Fig. 6

Linear Synchronous Motor Drive Using Intelligent Control

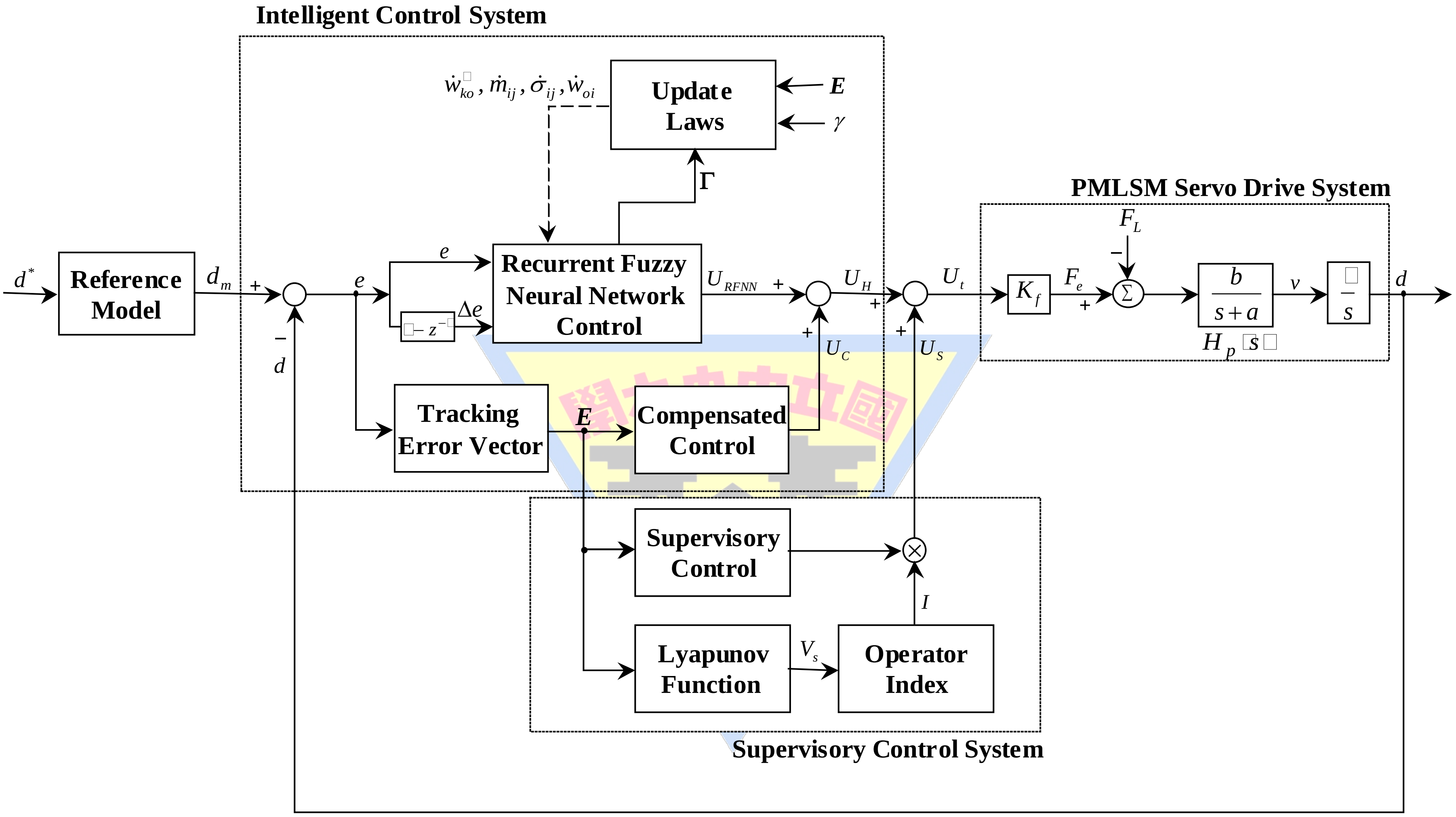

Fig. 7

Recurrent Fuzzy Neural Network

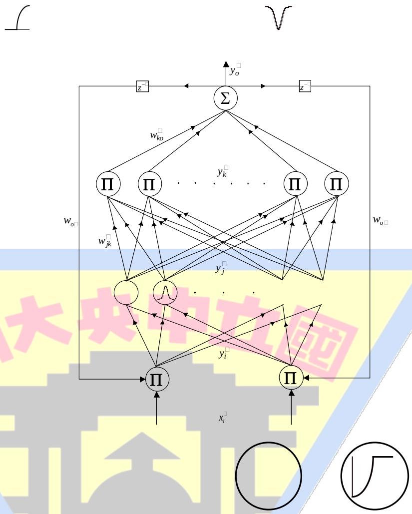

Output Layer o

Rule Layer k

Membership Layer j

Input Layer i

Fig. 8

Linear Synchronous Motor Drive Using Intelligent Control

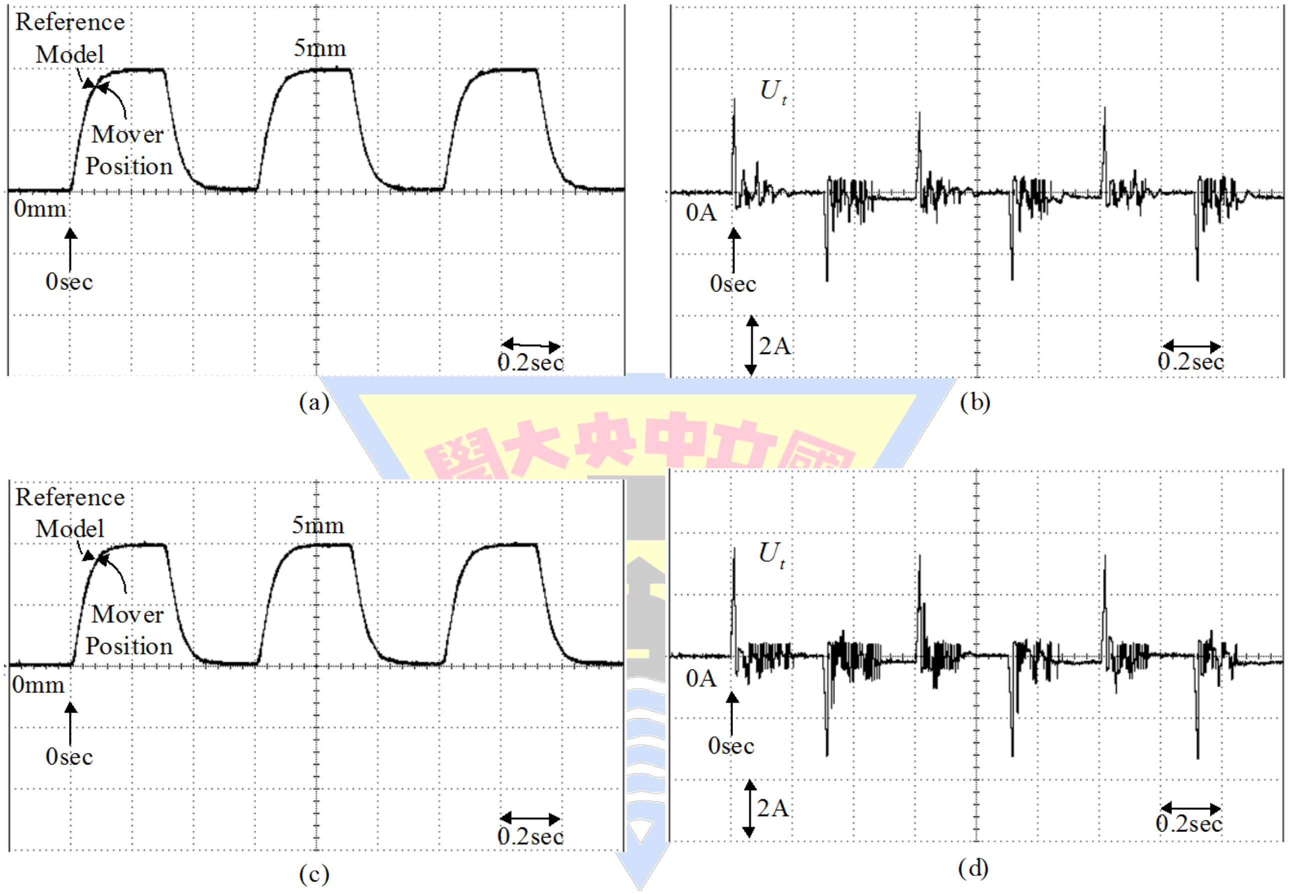

Fig. 9

Linear Synchronous Motor Drive Using Intelligent Control

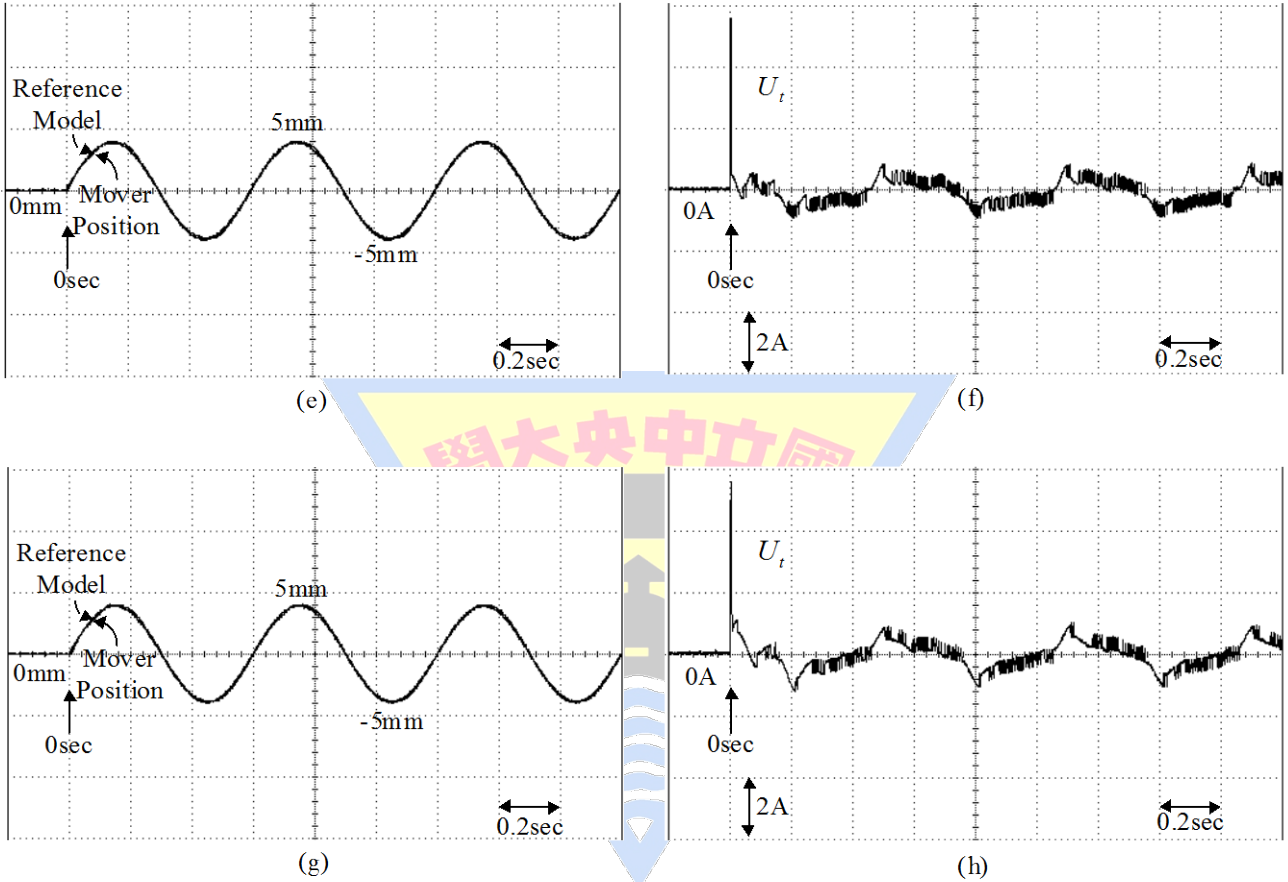

(e) (f)

(g) (h)

Fig. 9(續)

龍門式定位平台(Gantry)驅動控制系統

❒ 龍門式定位平台

本論文所使用之龍門式定位平台系統為上銀微系統股份有限公司所生產製造型號LMG2A-S13 S27的龍門式定位平台。

y軸是由二台的永磁線型同步馬達所組成的雙平行馬達系統；x軸是由一台永磁線型同步馬達組成。

- y軸型號：LMS 27
  x軸型號：LMS 13
- y軸最大行程：1000mm
  x軸最大行程：750mm
- 額定電壓：220V
  額定連續電流：5.0A
  連續推力：180N
  永磁極距為：3.2cm

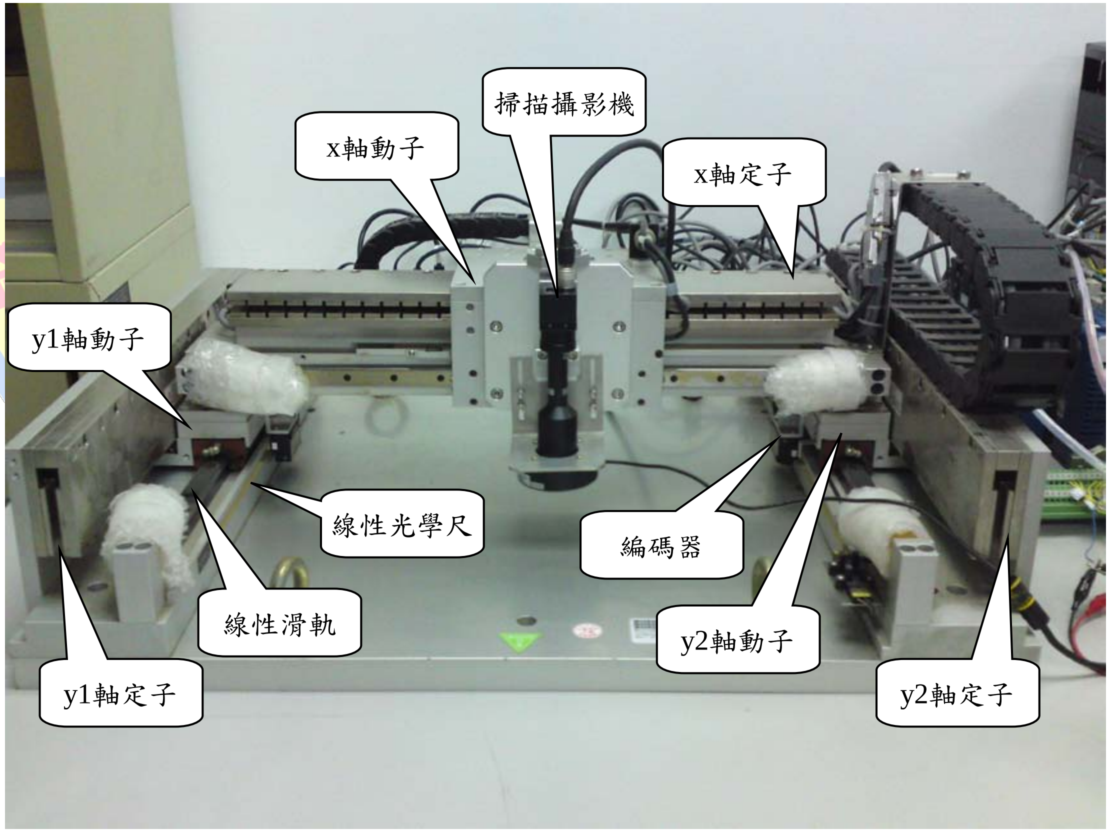

Fig. 10 龍門式定位平台控制系統

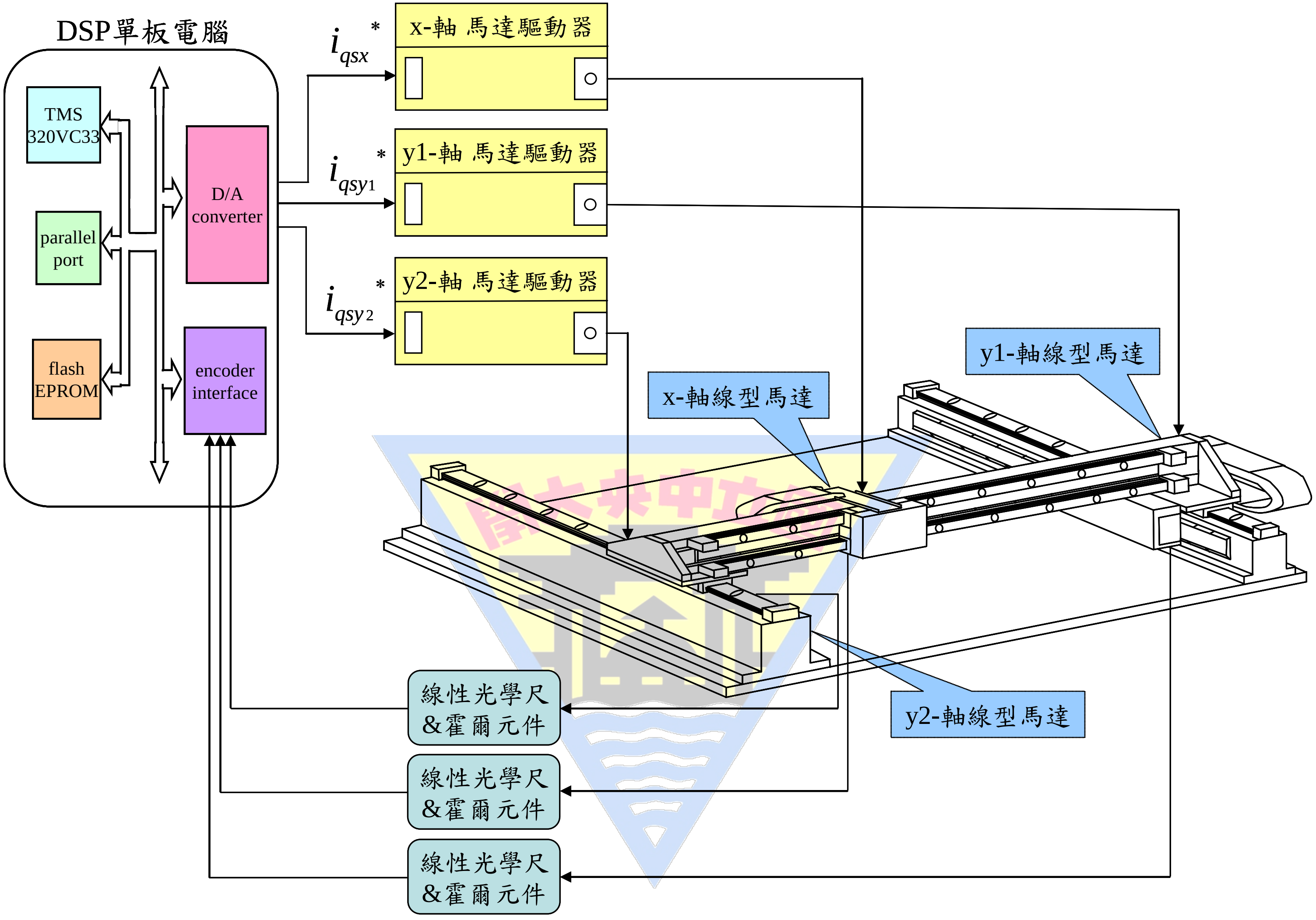

Fig. 11 龍門式定位平台控制系統方塊圖

- 互補式滑動模態控制器結合Sugeno型模糊類神經網路控制系統

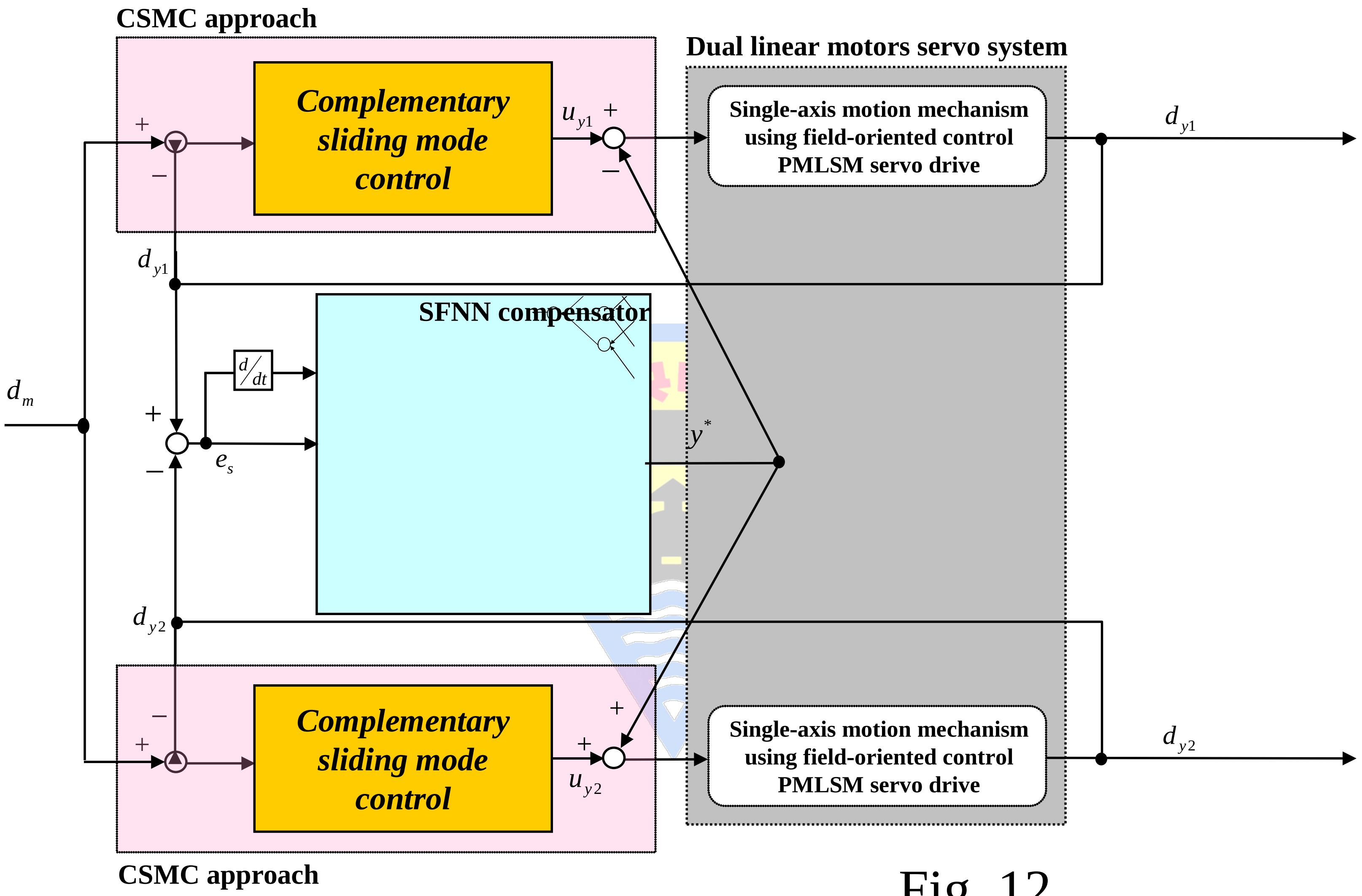

Fig. 12

龍門式定位平台(Ga

以**片段線性**模式為基礎，可將**非線性**系統**解構成局部線性**模式組合的一種建模架構，相較於Mamdani型有更佳的表達方式與更快的運算速度。

❒ Sugeno型模糊類神經網路

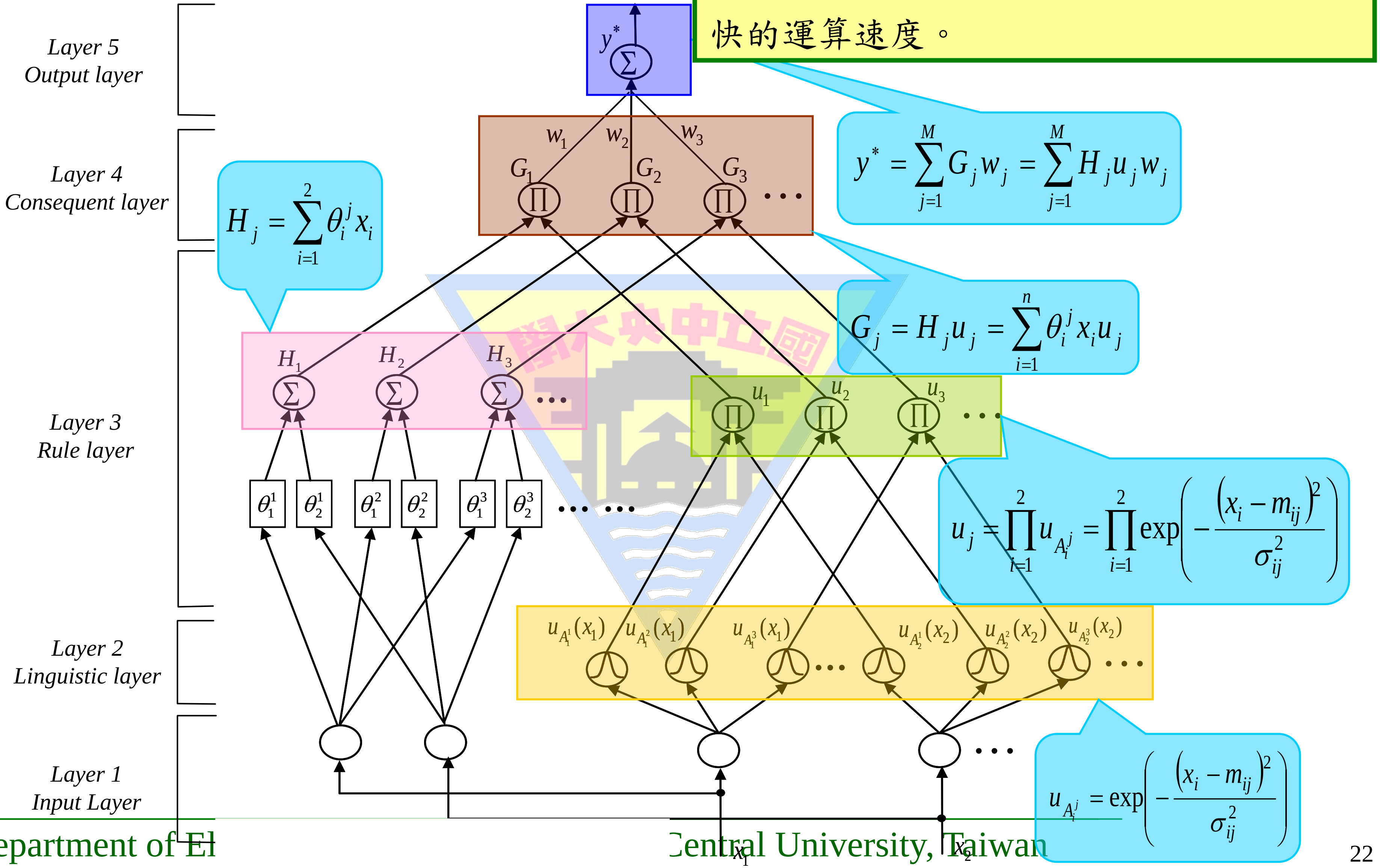

$$H_j = \sum_{i=1}^{2} \theta_i^j x_i$$

$$y^* = \sum_{j=1}^{M} G_j w_j = \sum_{j=1}^{M} H_j u_j w_j$$

$$G_j = H_j u_j = \sum_{i=1}^{n} \theta_i^j x_i u_j$$

$$u_j = \prod_{i=1}^{2} u_{A_i^j} = \prod_{i=1}^{2} \exp\left(-\frac{(x_i - m_{ij})^2}{\sigma_{ij}^2}\right)$$

$$u_{A_i^j} = \exp\left(-\frac{(x_i - m_{ij})^2}{\sigma_{ij}^2}\right)$$

互補式滑動模態控制器結合比例微分控制器控制系統

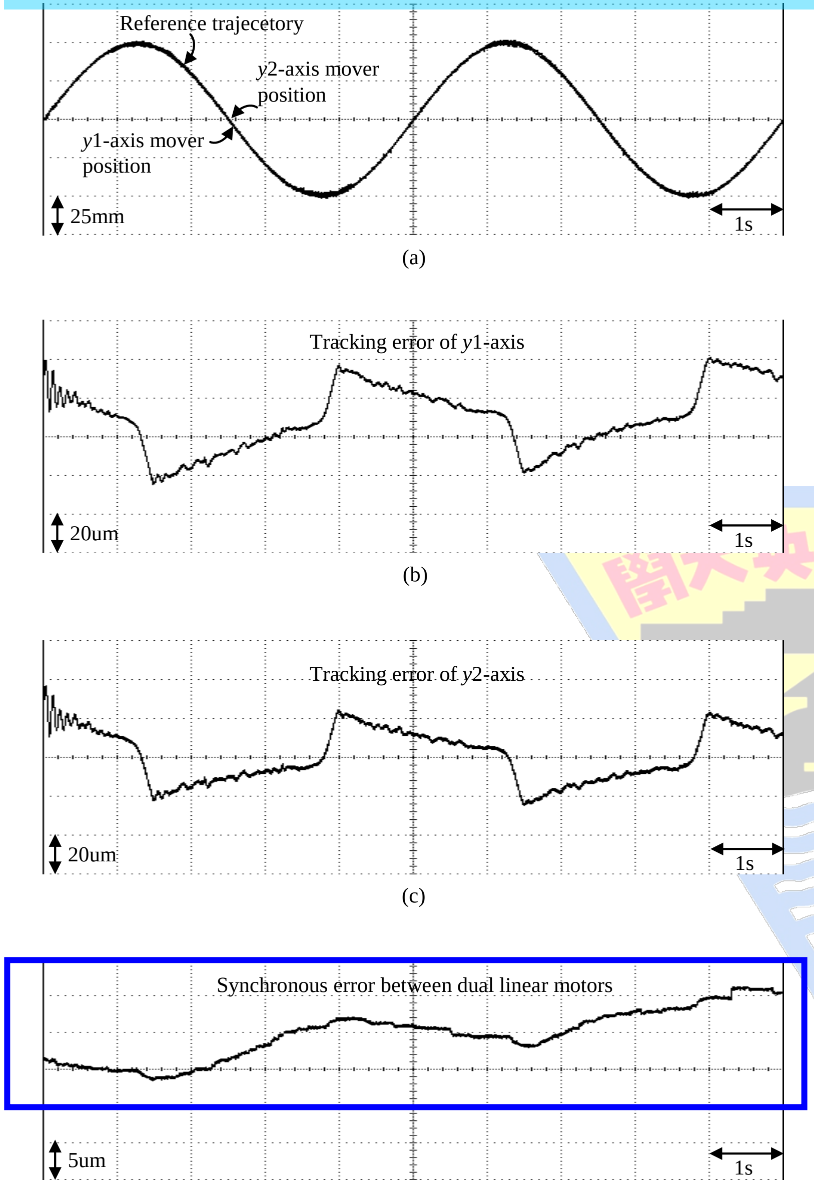

(a) (b) (c) (d)

互補式滑動模態控制器結合Sugeno型模糊類神經網路控制系統

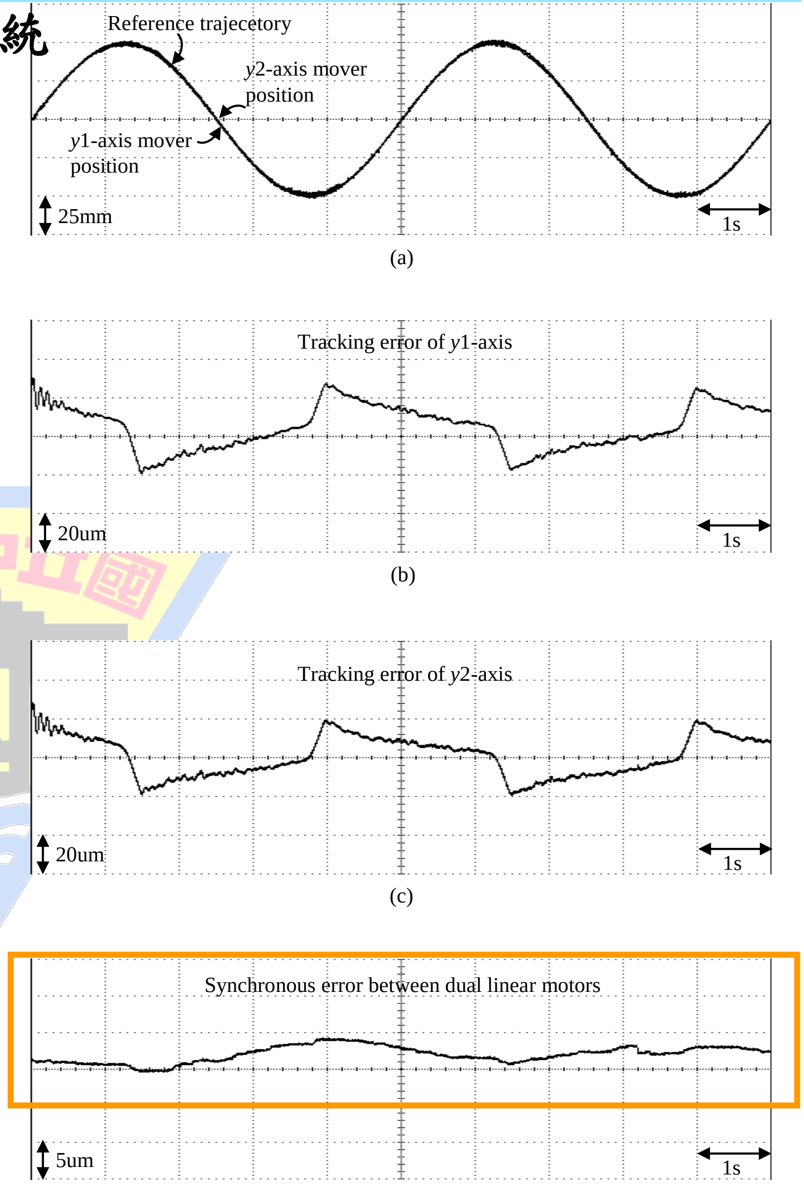

(a) (b) (c) (d)

Fig. 13

龍門式定位平台(Gantry)驅動控制系統

❒ 傳統耦合同動控制策略

雙線性馬達系統之閉迴路穩定性無法保證

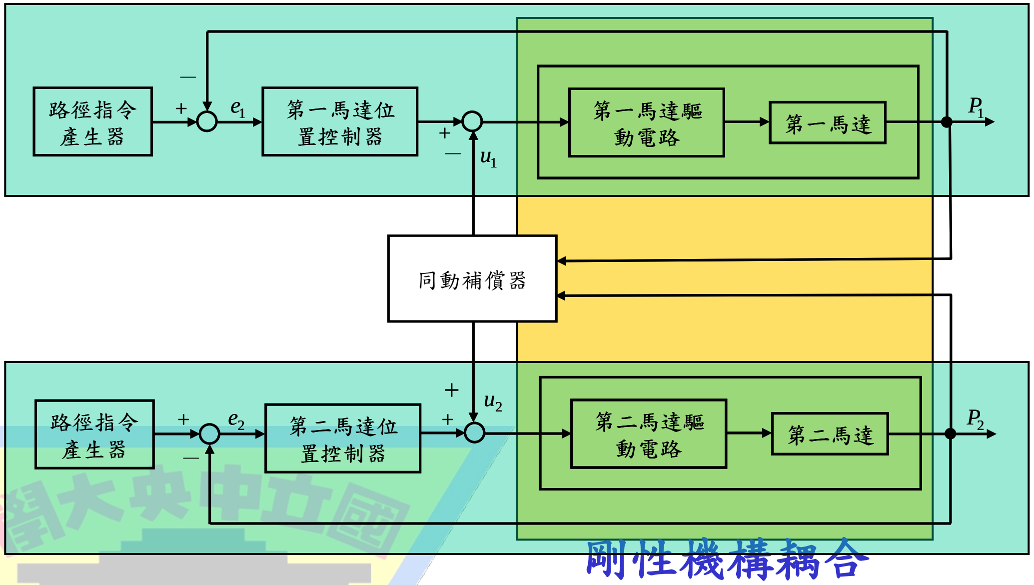

❒ 交叉耦合同動控制策略

雙線性馬達系統之閉迴路穩定性可以保證

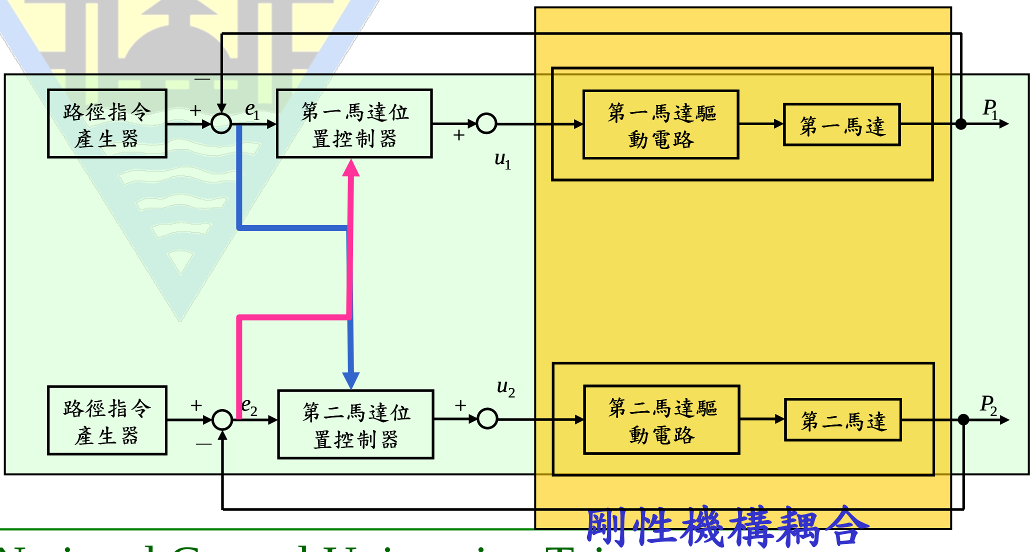

龍門式定位平台(Gantry)驅動控制系統

- 交叉耦合式函數連結放射狀基底函數網路控制系統

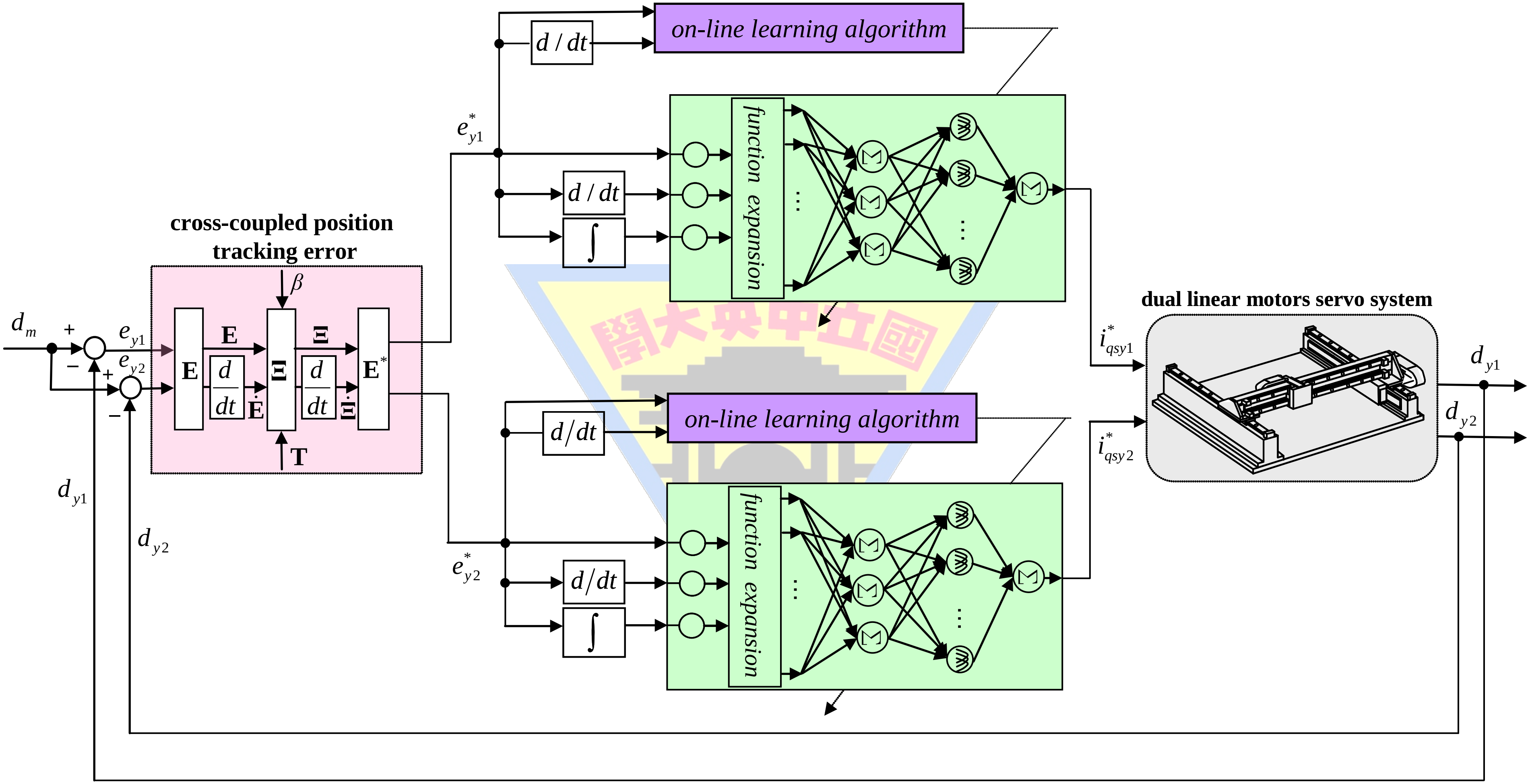

Fig. 14

龍門式定位平台(Gantry)驅動控制系統

❐ 函數連結放射狀基底函數網路控制系統

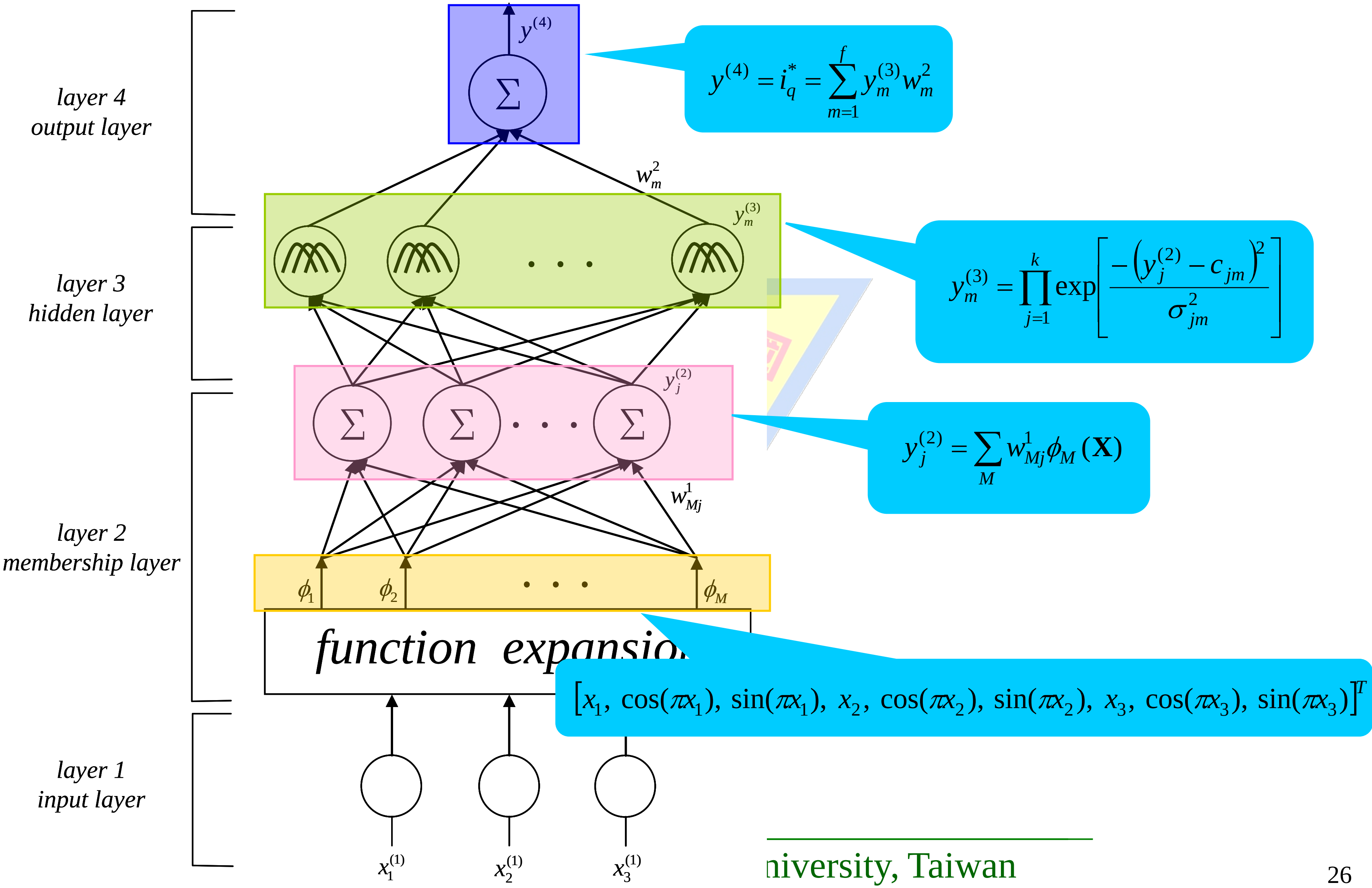

$$y^{(4)} = i_q^* = \sum_{m=1}^{f} y_m^{(3)} w_m^2$$

$$y_m^{(3)} = \prod_{j=1}^{k} \exp\left[\frac{-\left(y_j^{(2)} - c_{jm}\right)^2}{\sigma_{jm}^2}\right]$$

$$y_j^{(2)} = \sum_M w_{Mj}^1 \phi_M(\mathbf{X})$$

$$[x_1,\ \cos(\pi x_1),\ \sin(\pi x_1),\ x_2,\ \cos(\pi x_2),\ \sin(\pi x_2),\ x_3,\ \cos(\pi x_3),\ \sin(\pi x_3)]^T$$

龍門式定位平台(Gantry)驅動控制系統

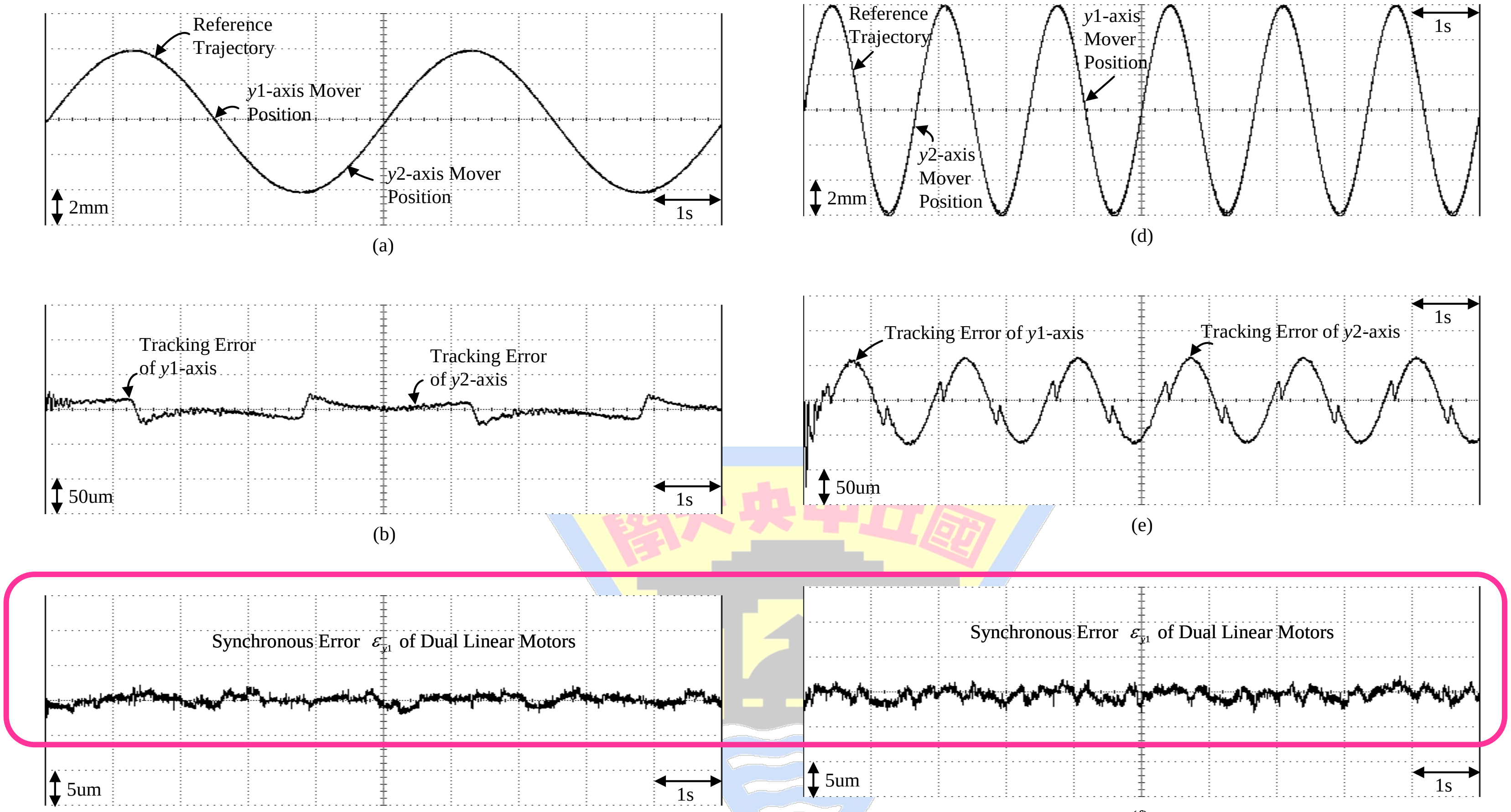

(a) (b) (c) (d) (e) (f)

Case1

Case2

	週期性弦波命令		負載
	頻率	振幅	
Case1	0.2Hz	4mm	0kg
Case2	0.6Hz	6mm	7.32kg

Fig. 15

Five-degree-of-freedom Active Magnetic Bearing (AMB)

- The elements of AMB:
  - Electromagnet
  - Rotor
  - Sensor
  - Controller
  - Power Amplifier

What is AMB?

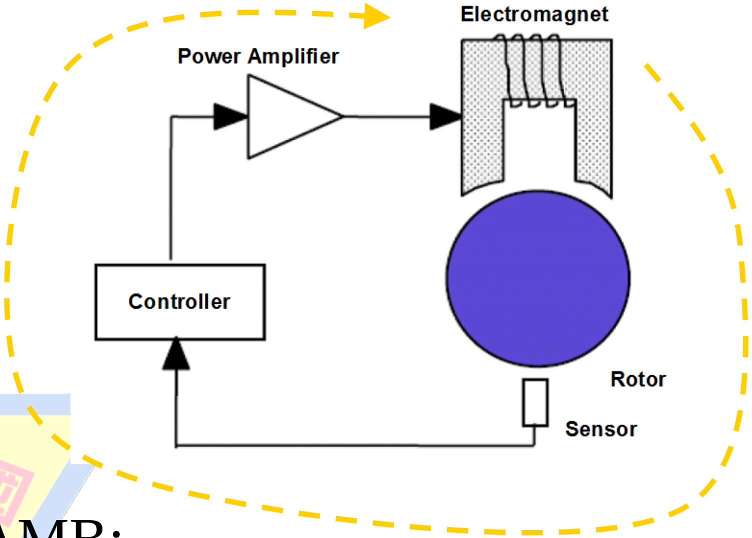

- According to its structure and usage of AMB:
  - Radial AMB (RAMB)
  - Thrust AMB (TAMB), i.e. Axial AMB
  - Combination

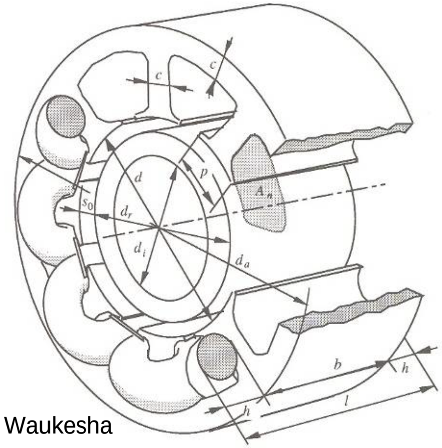

Source: Schweitzer, Waukesha

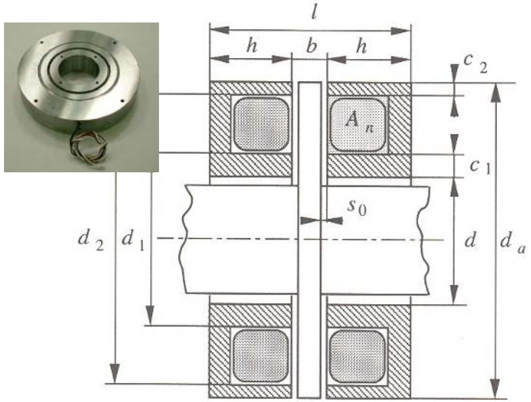

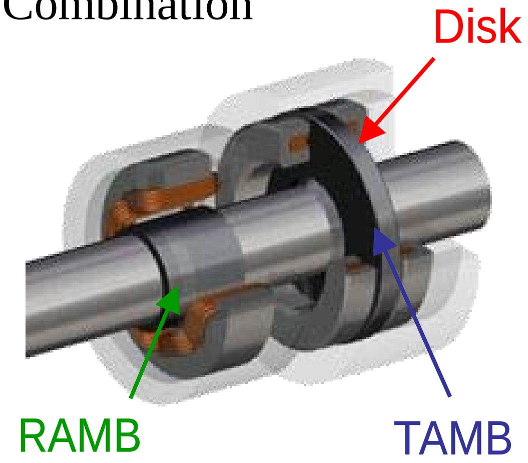

System Dissection, Dynamic Analyses and Experimental Designs of Five-DOF AMB System

- The fully suspended five-DOF AMB system is composed of four radial DOF controlled by two identical RAMBs and one axial DOF controlled by a TAMB.

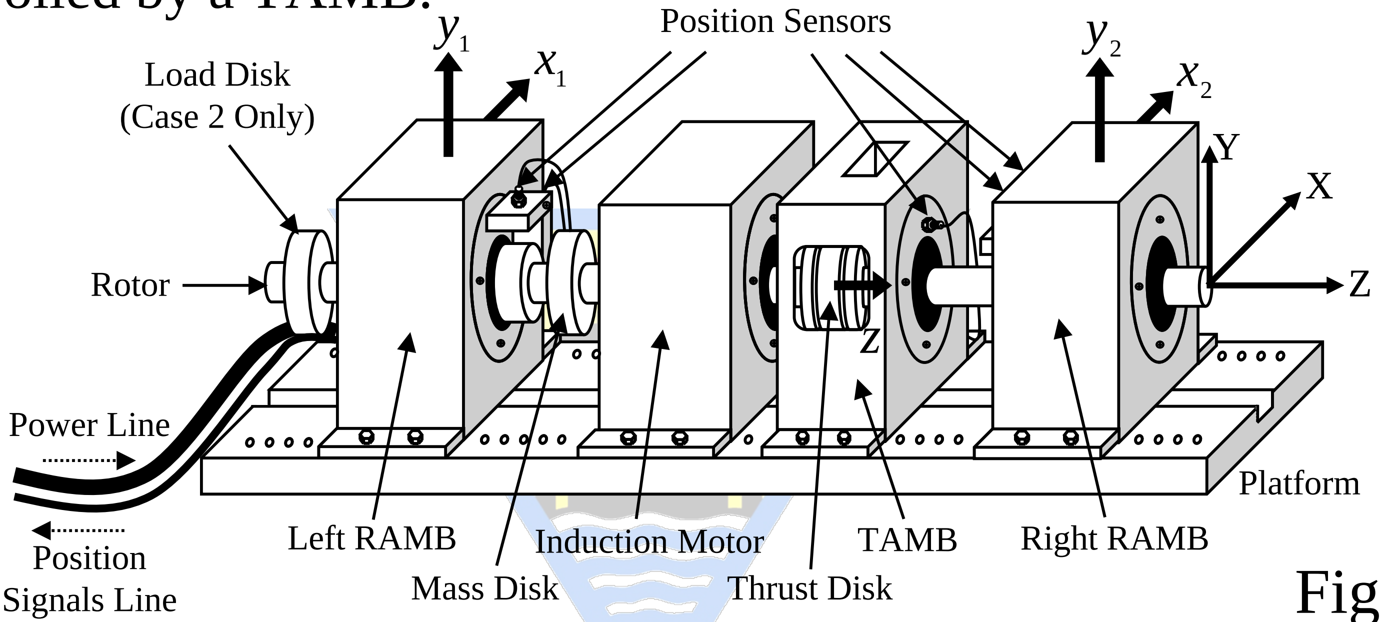

Fig. 16

System Dissection, Dynamic Analyses, and Experimental Designs of Five-DOF AMB System

- In the case of an AMB, where iron is used in the stator and the rotor, electromagnets cause a flux Φ to circulate a magnetic loop.
- The relation of flux Φ and cross-sections A_s and A_0 can be stated as

$$\Phi = B_s A_s = B_0 A_0$$

- One can obtain the following result

$$B_0 = \frac{\Phi_0}{A} = \frac{Ni}{\left(\cancelto{0}{\frac{l_s}{\mu_s}} + \cancelto{0}{\frac{l_r}{\mu_r}} + \frac{2l_0}{\mu_0}\right)} \cong \frac{\mu_0 Ni}{2l_0}$$

- Consider the Maxwell force

$$f = \frac{B_0^2 A_0}{\mu_0} = \frac{\mu_0 A_0 N^2 i^2}{4l_0^2} = k\frac{i^2}{l_0^2}$$

quadratic!

inversely quadratic!

where $k = \dfrac{\mu_0 A_0 N^2}{4}$

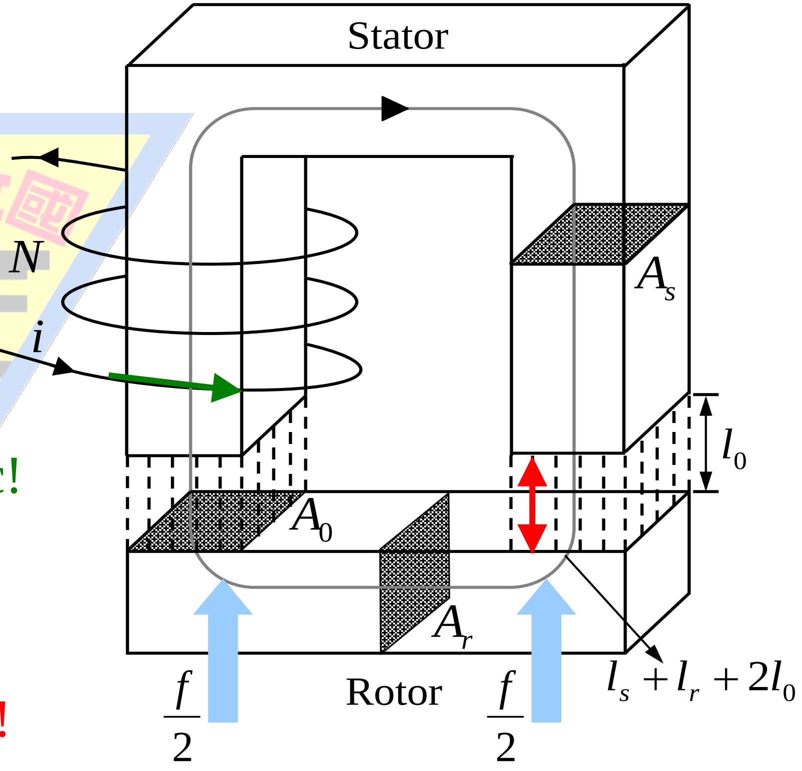

Robust Control of Fully Suspended Five-DOF AMB System Using Decentralized PIDNN Control

- The network structure of the PIDNN controller used for φ-axis of the five-DOF AMB system is shown as:

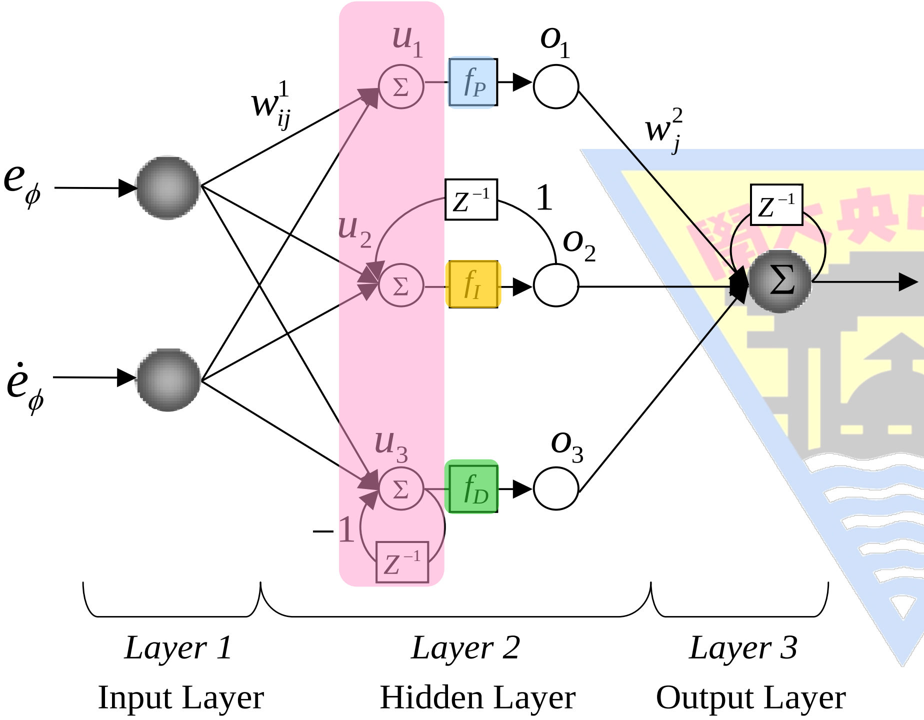

Fig. 17

P control

$$o_1(N) = f_P\big(u_1(N)\big) = \sum_{i=1}^{2} w_{i1}^1(N)\phi_i(N)$$

I control

$$o_2(N) = f_I\big(u_2(N) + o_2(N-1)\big) = \sum_{i=1}^{2} w_{i2}^1(N)\phi_i(N) + o_2(N-1)$$

D control

$$o_3(N) = f_D\big(u_3(N) - u_3(N-1)\big) = \sum_{i=1}^{2} w_{i3}^1(N)\phi_i(N) - \sum_{i=1}^{2} w_{i3}^1(N-1)\phi_i(N-1)$$

Robust Control of Fully Suspended Five-DOF AMB System Using Decentralized PIDNN Control

- Te on-line learning algorithm of the PIDNN using supervised gradient decent method:

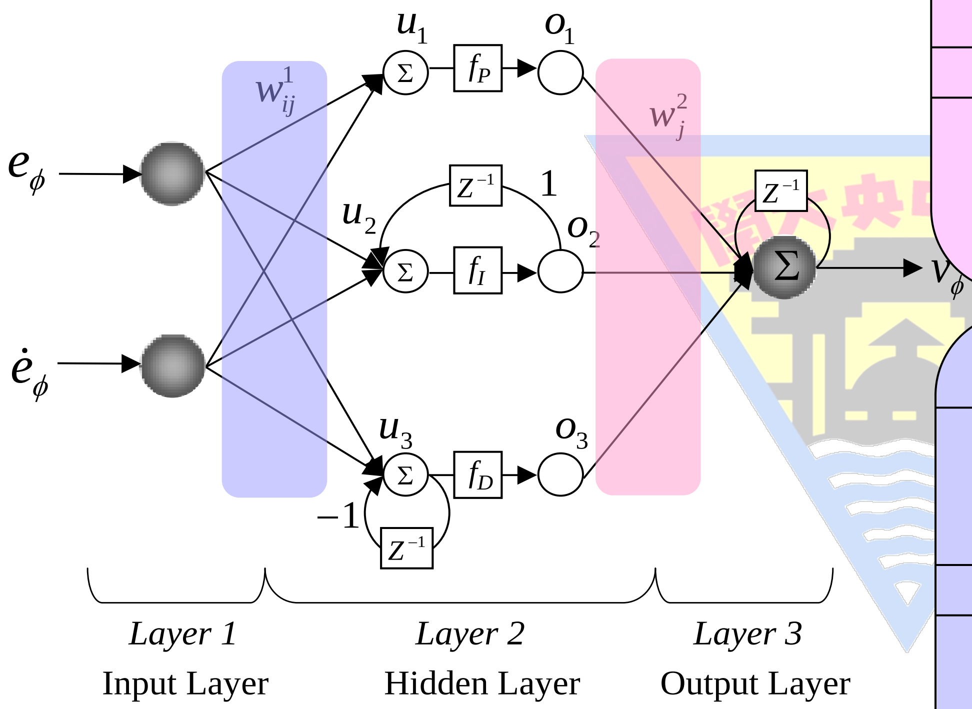

Connective Weight Between Hidden and Output Layers

$$\Delta w_j^2(N) = -\eta_{W^2}\frac{\partial E(N)}{\partial w_j^2(N)} = \eta_{W^2}\delta_\phi(N)o_j(N)$$

$$w_j^2(N+1) = w_j^2(N) + \Delta w_j^2(N)$$

Optimal Learning Rate

$$\eta_{W^2} = \frac{E(N)}{2\left\{\sum_{j=1}^{3}\left[\frac{\partial E(N)}{\partial w_j^2}\right]^2 + \varepsilon\right\}}$$

Connective Weight Between Input and Hidden Layers

$$\Delta w_{ij}^1(N) = -\eta_{W^1}\frac{\partial E(N)}{\partial w_{ij}^1(N)} = \eta_{W^1}\delta_\phi(N)w_j^2(N)\phi_i(N)$$

$$w_{ij}^1(N+1) = w_{ij}^1(N) + \Delta w_{ij}^1(N)$$

Optimal Learning Rate

$$\eta_{W^1} = \frac{E(N)}{2\left\{\sum_{i=1}^{2}\sum_{j=1}^{3}\left[\frac{\partial E(N)}{\partial w_{ij}^1}\right]^2 + \varepsilon\right\}}$$

$$E(N+1) = \frac{1}{2}e_\phi{}^2(N+1) < E(N)$$

Robust Control of Fully Suspended Five-DOF AMB System Using Decentralized PIDNN Control

- The configuration of the ψ-axis AMB control subsystem using PIDNN controller with on-line learning algorithm and adaptive learning rates is shown as follows:

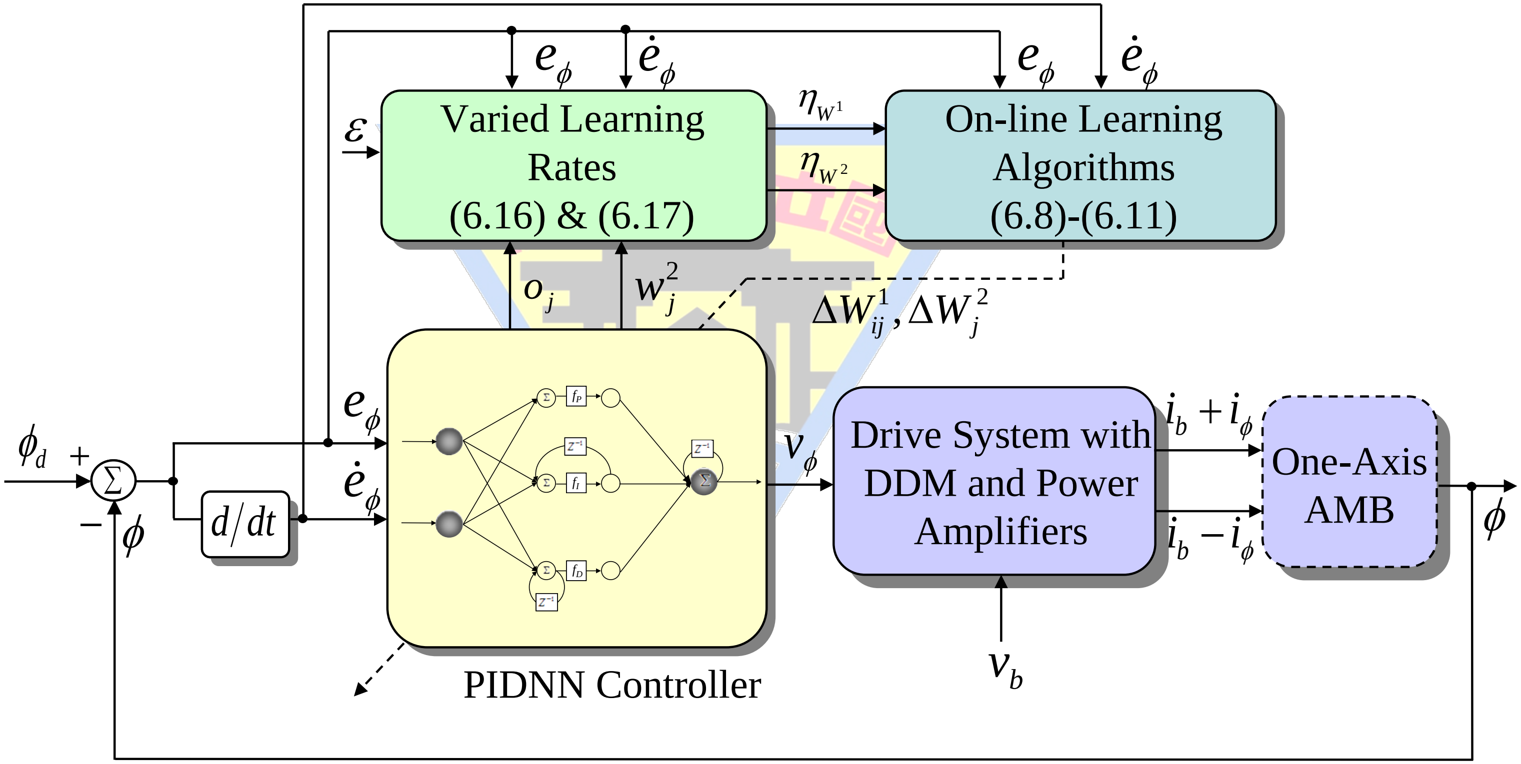

Fig. 18

Robust Control of Fully Suspended Five-DOF AMB System Using Decentralized PIDNN Control

- *A. Experimental results of fully suspended five-DOF AMB control system using decentralized PID controller*
  - Five conventional PID controllers are also used to construct a decentralized PID controller for the comparison of control performances.

$$u_\phi = K_{P\phi} e_\phi + K_{I\phi} \int_0^t e_\phi dt + K_{D\phi} \dot{e}_\phi$$

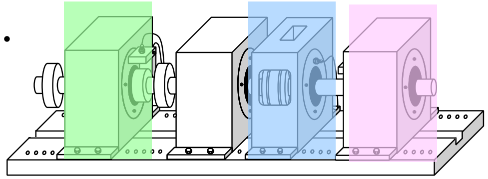

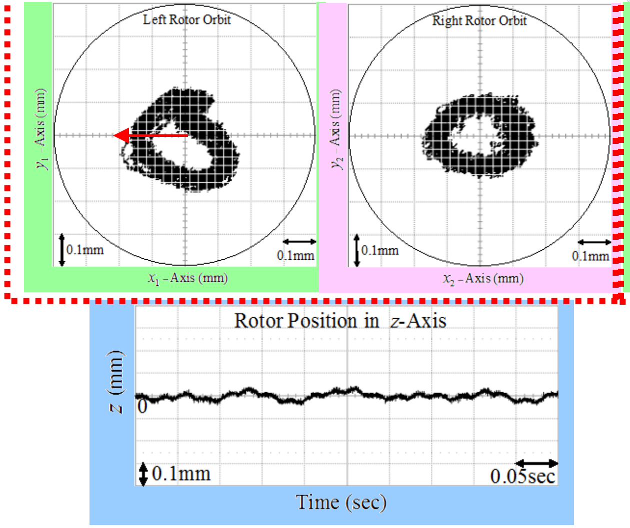
maximum run outs: 0.2 mm

Case 1
2400RPM

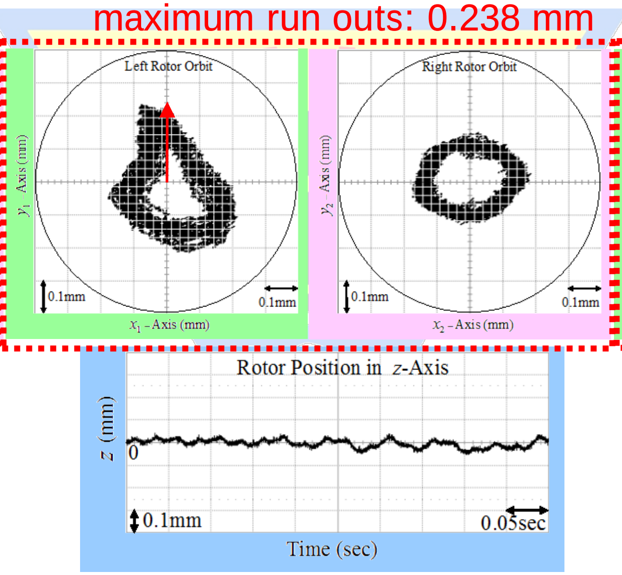
maximum run outs: 0.238 mm

Case2
2400RPM with Load

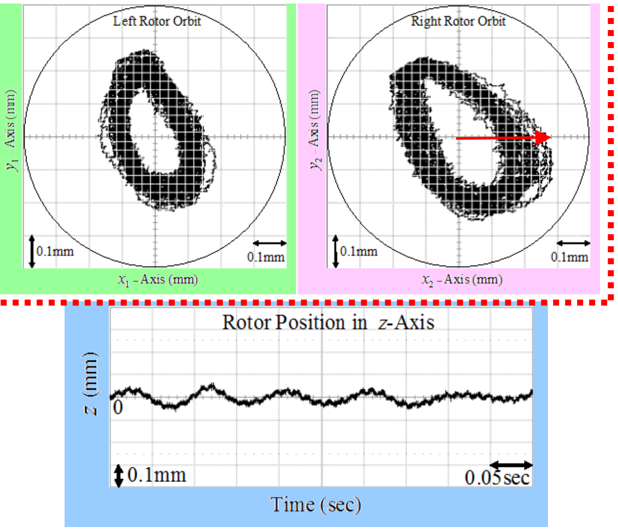
maximum run outs: 0.282 mm

Case 3
4800RPM

Robust Control of Fully Suspended Five-DOF AMB System Using Decentralized PIDNN Control

- *A. Experimental results of fully suspended five-DOF AMB control system using decentralized PIDNN controller*
  - Five proposed PIDNN controllers are used to construct a decentralized PIDNN controller to achieve the regulating and stabilizing purposes for the fully suspended five-DOF AMB control system.

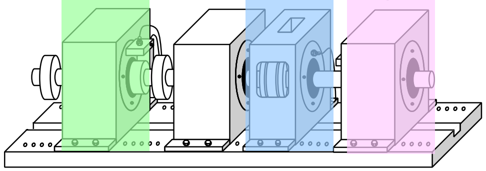

maximum run outs: 0.16 mm

maximum run outs: 0.19 mm

maximum run outs: 0.22 mm

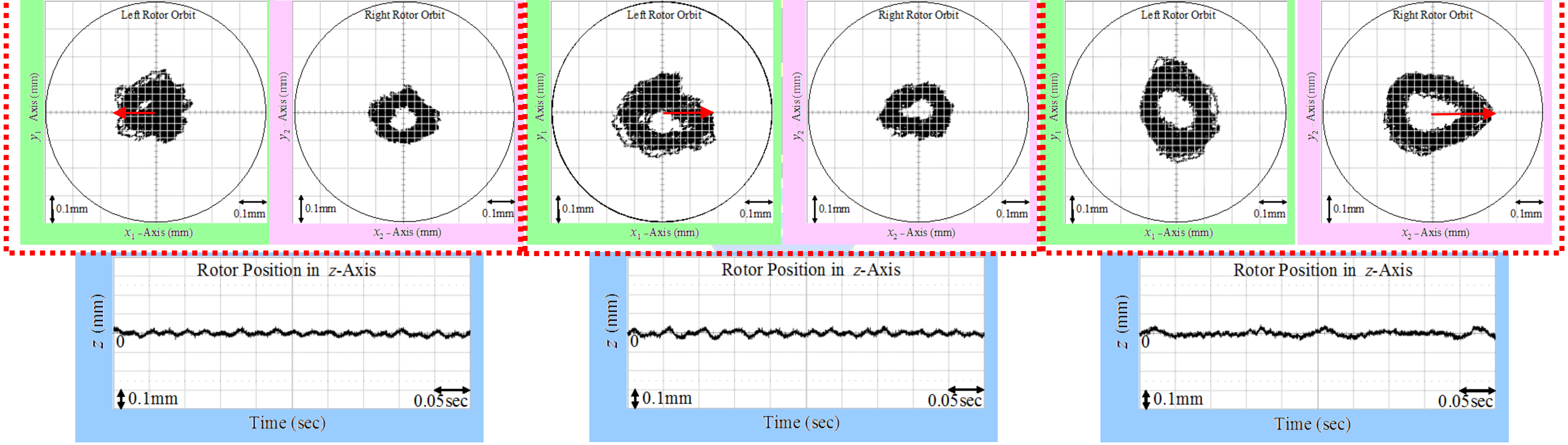

Case 1
2400RPM

Case2
2400RPM with Load

Case 3
4800RPM

Robust Control of Fully Suspended Five-DOF AMB System Using Decentralized PIDNN Control

- The performance measures of the decentralized PID controller, decentralized PIDNN controller are shown in the following.
- Obviously, the proposed decentralized PIDNN controller possesses the better robust control performance.

Axes	Regulating Errors (μm)	Case 1		Case 2		Case 3	
		PID	PIDNN	PID	PIDNN	PID	PIDNN
x_1	RMS Values	79.02	60.68	92.94	77.64	82.72	73.81
	Peak to Peak Values	359.1	278.7	390.5	373.3	356.0	286.5
y_1	RMS Values	88.39	50.85	114.09	72.38	130.60	87.62
	Peak to Peak Values	315.9	265.9	447.5	307.7	486.7	377.9
x_2	RMS Values	90.23	59.95	102.98	70.86	125.87	104.42
	Peak to Peak Values	351.1	259.8	358.8	276.4	495.1	389.0
y_2	RMS Values	66.54	52.00	73.29	46.71	148.03	74.75
	Peak to Peak Values	259.8	215.1	277.7	213.2	495.0	302.7
z	RMS Values	14.42	9.45	17.01	11.30	21.45	12.34
	Peak to Peak Values	84.7	66.3	93.7	75.6	126.8	83.2

Fault Tolerant Control of Six-Phase PMSM Drive System—Using TSKFNN-AMF Control

- Fault tolerant control six-phase PMSM drive system using TSKFNN-AMF control

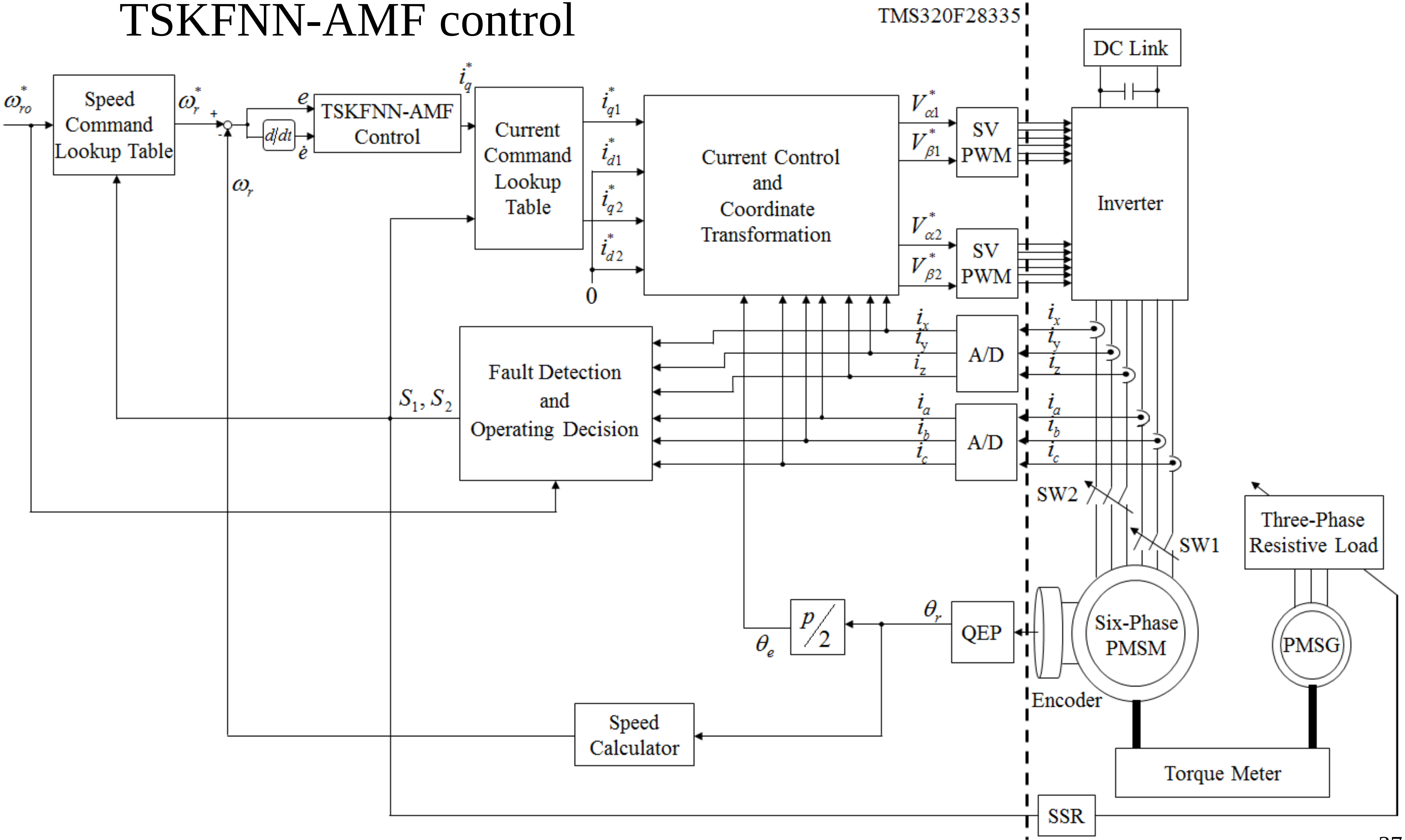

Fault Tolerant Control of Six-Phase PMSM Drive System—Using TSKFNN-AMF Control

- TSK type FNN with asymmetric membership function

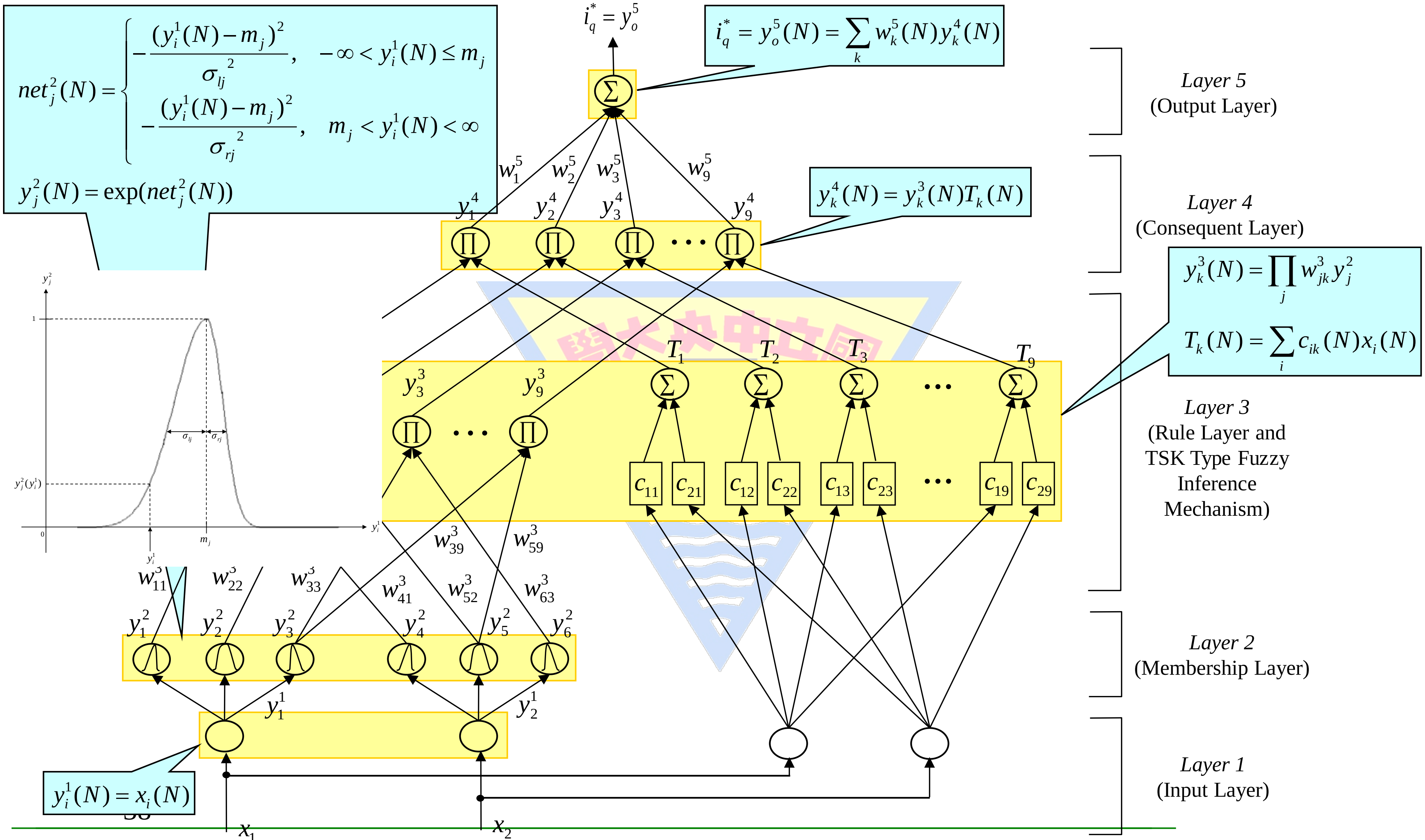

$$net_j^2(N)=\begin{cases}-\dfrac{(y_i^1(N)-m_j)^2}{\sigma_{lj}{}^2}, & -\infty<y_i^1(N)\le m_j\\ -\dfrac{(y_i^1(N)-m_j)^2}{\sigma_{rj}{}^2}, & m_j<y_i^1(N)<\infty\end{cases}$$

$$y_j^2(N)=\exp(net_j^2(N))$$

$$i_q^*=y_o^5(N)=\sum_k w_k^5(N)y_k^4(N)$$

$$y_k^4(N)=y_k^3(N)T_k(N)$$

$$y_k^3(N)=\prod_j w_{jk}^3 y_j^2$$

$$T_k(N)=\sum_i c_{ik}(N)x_i(N)$$

$$y_i^1(N)=x_i(N)$$

Fault Tolerant Control of Six-Phase PMSM Drive System—Using TSKFNN-AMF Control

- To obtain the leaning algorithm for the TSKFNN-AMF, the BP learning rule is adopted here. First, the energy function is defined as:

$$E = \frac{1}{2}(\omega_r^* - \omega_r)^2 = \frac{1}{2}e^2 \qquad (4.9)$$

- Then, the update laws are:

$$\Delta w_k^5 = -\eta_w \frac{\partial E}{\partial w_k^5} = -\eta_w \frac{\partial E}{\partial y_o^5(N)} \frac{\partial y_o^5(N)}{\partial w_k^5} = \eta_w \delta_o^5 y_k^4 \qquad (4.11)$$

$$\Delta c_{ik} = -\eta_c \frac{\partial E}{\partial c_{ik}} = -\eta_c \frac{\partial E}{\partial y_o^5(N)} \frac{\partial y_o^5(N)}{\partial y_k^4(N)} \frac{\partial y_k^4(N)}{\partial T_k(N)} \frac{\partial T_k(N)}{\partial c_{ik}(N)} = \eta_c \delta_k^4 y_k^3 x_i \qquad (4.15)$$

$$\begin{aligned}
\Delta m_j &= -\eta_m \frac{\partial E}{\partial m_j(N)} \\
&= -\eta_m \frac{\partial E}{\partial y_o^5(N)} \frac{\partial y_o^5(N)}{\partial y_k^4(N)} \frac{\partial y_k^4(N)\partial y_k^3(N)}{\partial y_k^3(N)\partial y_j^2(N)} \frac{\partial y_j^2(N)}{\partial net_j^2(N)} \frac{\partial net_j^2(N)}{\partial m_j(N)} \qquad (4.18) \\
&= \begin{cases} \eta_m \delta_j^2 \dfrac{2(y_i^1 - m_j)}{\sigma_{lj}{}^2}, & -\infty < y_i^1 \le m_j \\[2ex] \eta_m \delta_j^2 \dfrac{2(y_i^1 - m_j)}{\sigma_{rj}{}^2}, & m_j < y_i^1 < \infty \end{cases}
\end{aligned}$$

Fault Tolerant Control of Six-Phase PMSM Drive System—Using TSKFNN-AMF Control

$$\Delta\sigma_{lj} = -\eta_{l\sigma}\frac{\partial E}{\partial\sigma_{lj}(N)}$$

$$= -\eta_{l\sigma}\frac{\partial E}{\partial y_o^5(N)}\frac{\partial y_o^5(N)}{\partial y_k^4(N)}\frac{\partial y_k^4(N)\partial y_k^3(N)}{\partial y_k^3(N)\partial y_j^2(N)}\frac{\partial y_j^2(N)}{\partial net_j^2(N)}\frac{\partial net_j^2(N)}{\partial\sigma_{lj}(N)} \qquad (4.19)$$

$$= \eta_{l\sigma}\delta_j^2\frac{2(y_i^1 - m_j)^2}{\sigma_{lj}{}^3}$$

$$\Delta\sigma_{rj} = -\eta_{r\sigma}\frac{\partial E}{\partial\sigma_{rj}(N)}$$

$$= -\eta_{r\sigma}\frac{\partial E}{\partial y_o^5(N)}\frac{\partial y_o^5(N)}{\partial y_k^4(N)}\frac{\partial y_k^4(N)\partial y_k^3(N)}{\partial y_k^3(N)\partial y_j^2(N)}\frac{\partial y_j^2(N)}{\partial net_j^2(N)}\frac{\partial net_j^2(N)}{\partial\sigma_{rj}(N)} \qquad (4.20)$$

$$= \eta_{r\sigma}\delta_j^2\frac{2(y_i^1 - m_j)^2}{\sigma_{rj}{}^3}$$

- The exact calculation of the sensitivity of the system, $\partial\omega_r / \partial y_o^5(N)$, is difficult to be determined due to the uncertainties and unmodeled dynamics of the six-phase PMSM drive system. The error term shown in (4.10) is assumed to approximate as follows:

$$\delta_o^5 \cong (\omega_r^* - \omega_r) + (\dot{\omega}_r^* - \dot{\omega}_r) = e + \dot{e} \qquad (4.24)$$

Fault Tolerant Control of Six-Phase PMSM Drive System—Using TSKFNN-AMF Control

- Healthy condition in experiment:
  - Periodical trapezoidal wave (0.056Hz) reference speed profile.
    - Y-connected three-phase resistive load 7Ω for the PMSG (Case 1)
    - Y-connected three-phase resistive load 3.5Ω for the PMSG (Case 2)

- Faulty condition in experiment:
  - Speed profile is set as 2250rpm at the beginning and reduced to half of the speed after three seconds when the fault detected. The three-phase resistive load will also be changed from 3.5Ω to 7Ω immediately by using the SSR when the fault is detected, and then changed to 3.5Ω after six seconds.
    - *abc* winding open (Case 3)
    - *xyz* winding open (Case 4)

Fault Tolerant Control of Six-Phase PMSM Drive System—Using TSKFNN-AMF Control

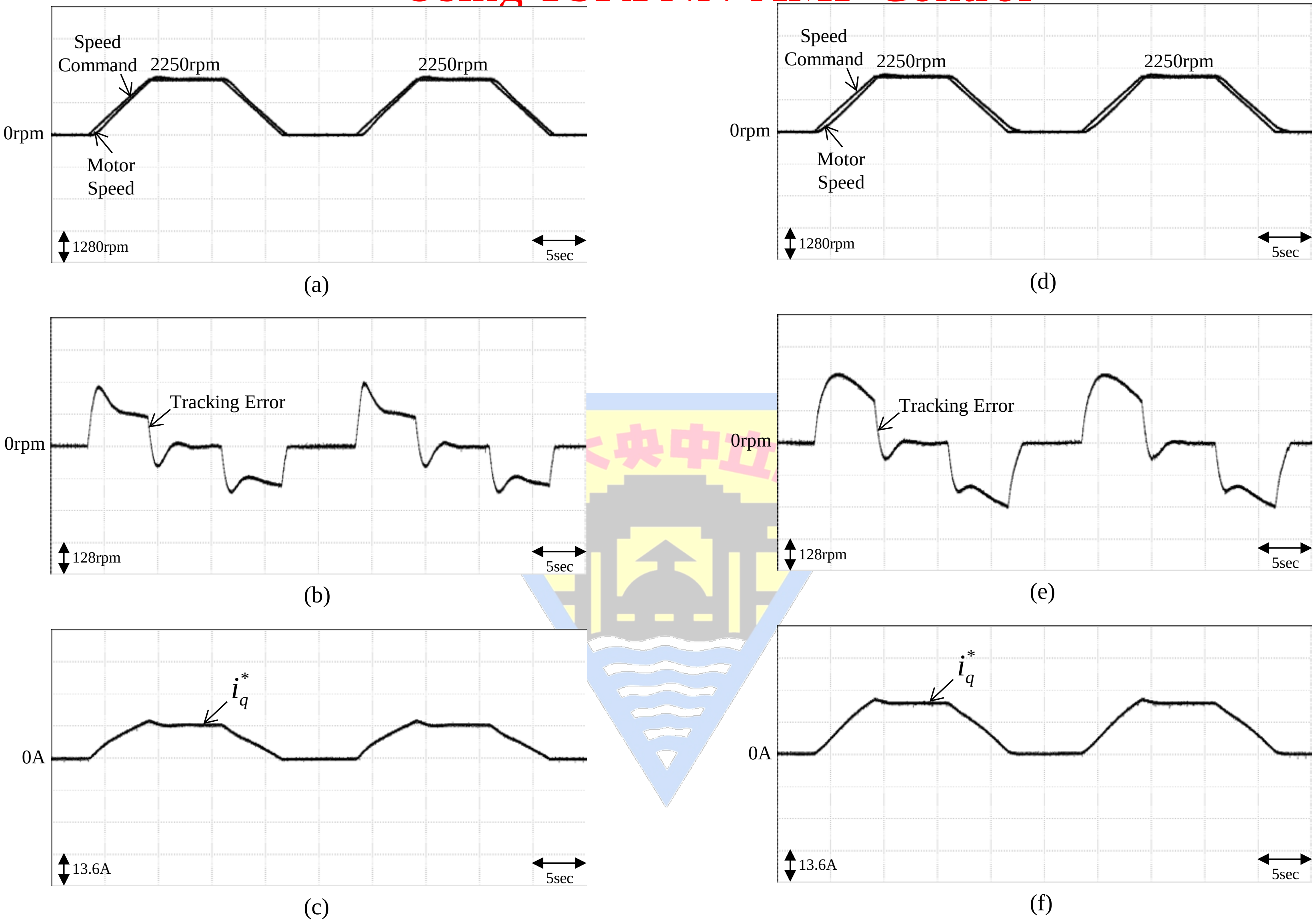

(a) (b) (c) (d) (e) (f)

Experimental results of PI control at Case 1(left) and Case 2(right)

Fault Tolerant Control of Six-Phase PMSM Drive System—Using TSKFNN-AMF Control

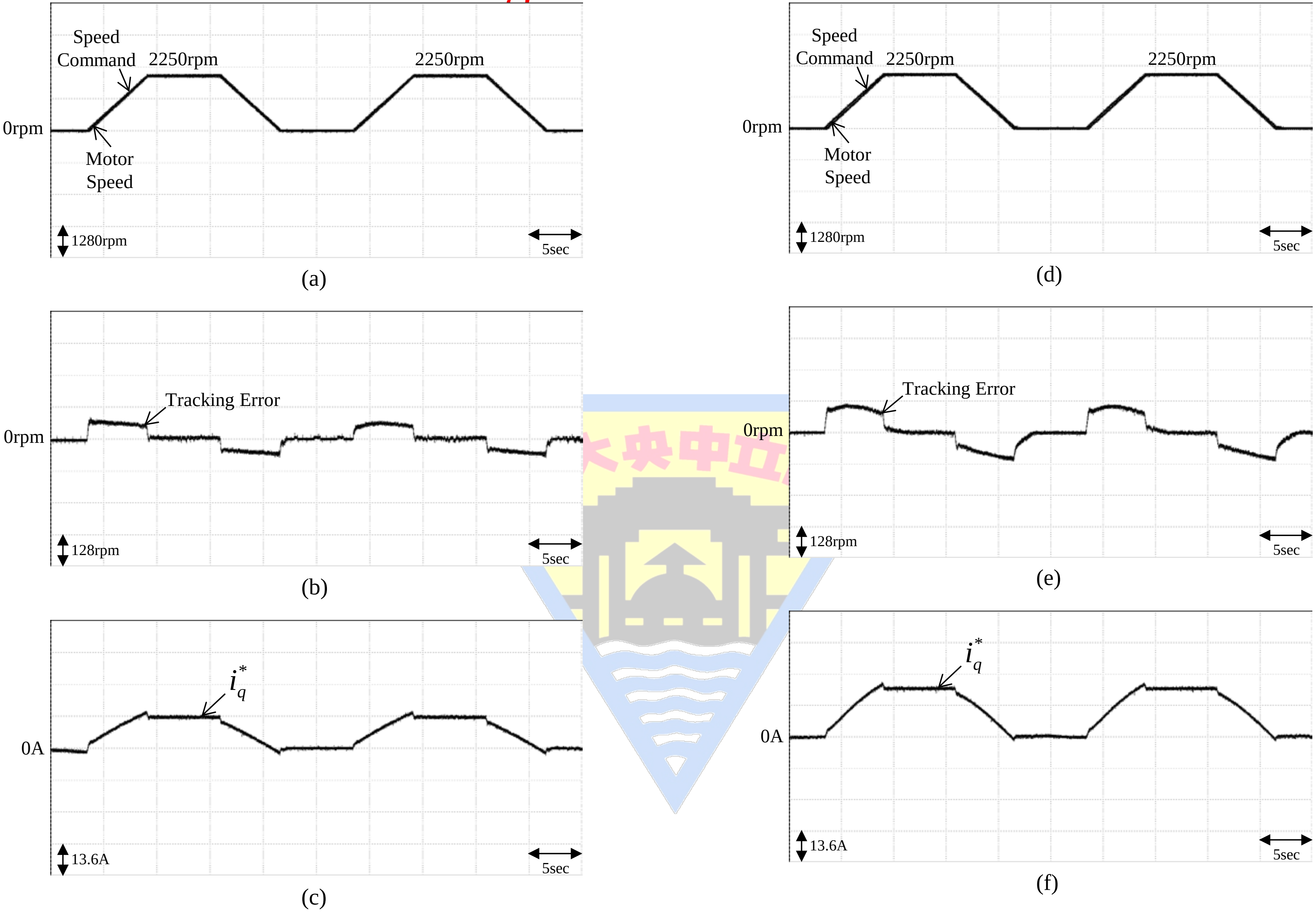

Experimental results of TSKFNN-AMF control at Case 1(left) and Case 2(right)

Fault Tolerant Control of Six-Phase PMSM Drive System— Using TSKFNN-AMF Control

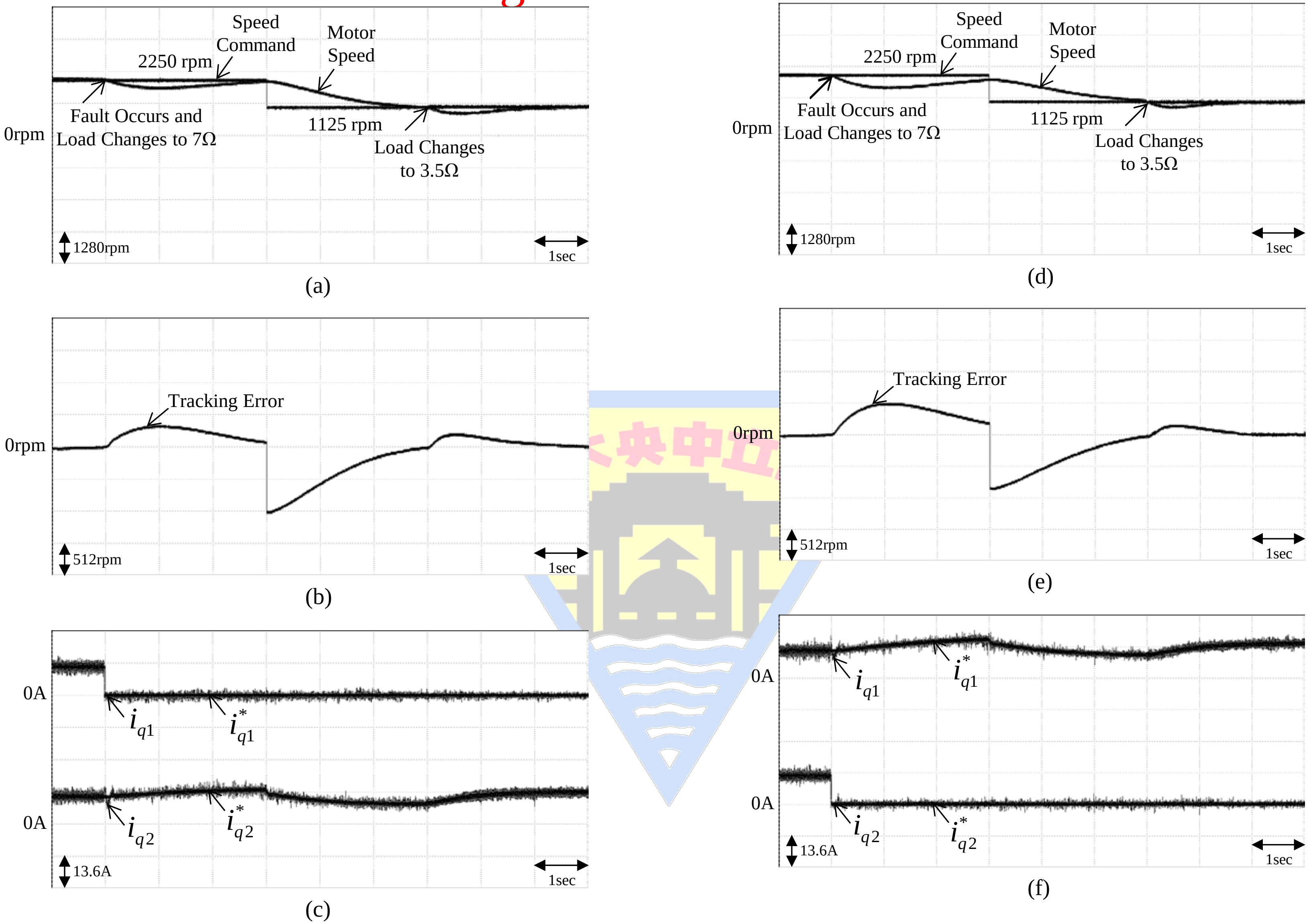

Experimental results of PI fault tolerant control at Case 3(left) and Case 4(right)

Fault Tolerant Control of Six-Phase PMSM Drive System—Using TSKFNN-AMF Control

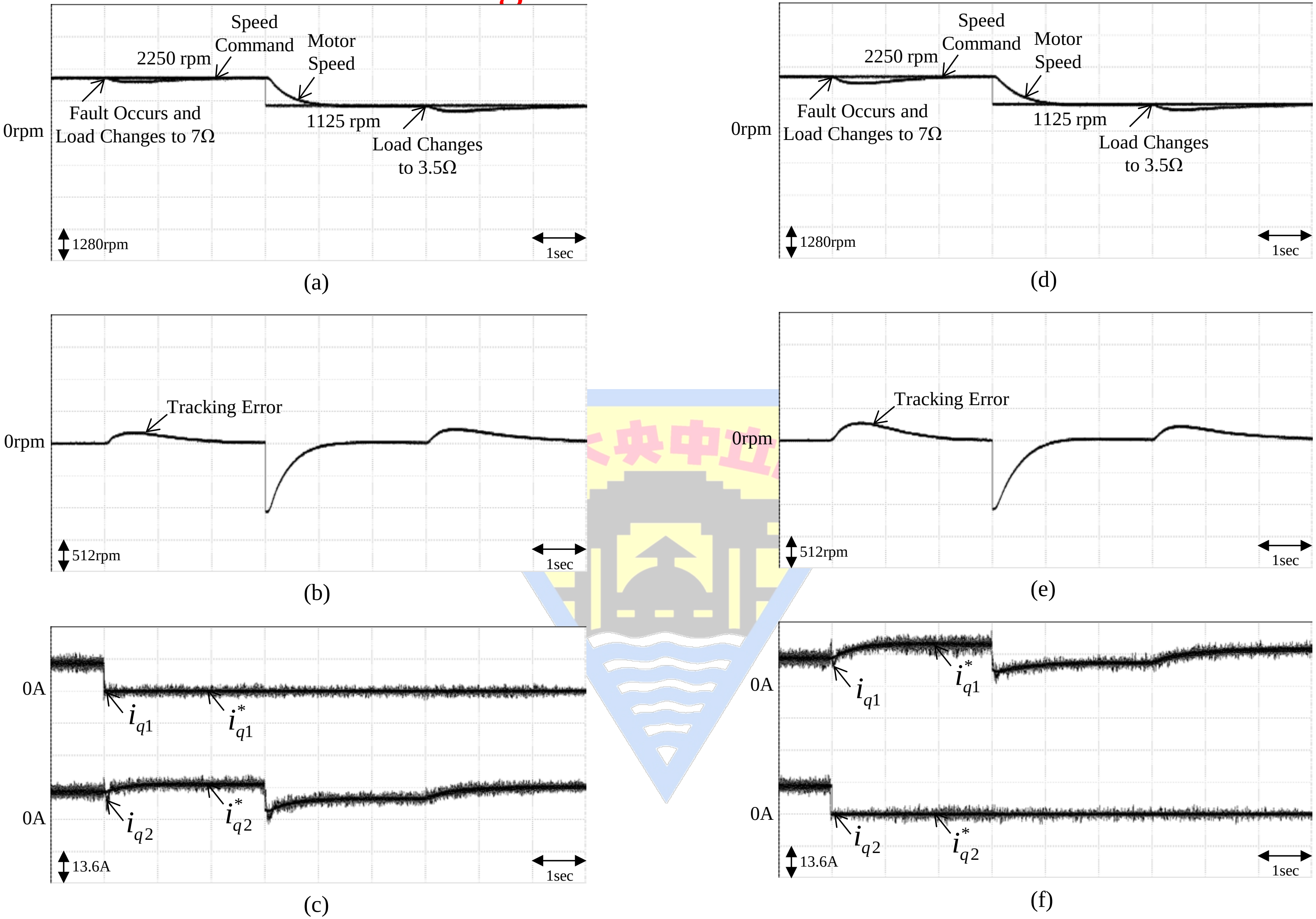
(a) (b) (c) (d) (e) (f)

Experimental results of TSKFNN-AMF fault tolerant control at Case 3(left) and Case 4(right)

Fault Tolerant Control of Six-Phase PMSM Drive System—Using TSKFNN-AMF Control

- The performance measurings of the PI and the proposed TSKFNN-AMF controls under healthy (Cases 1 and 2) and faulty (Cases 3 and 4) conditions are shown in Table 4.1 and Table 4.2 respectively.
- The proposed fault detection and operating decision method can detect the open phases of the motor effectively.

Table 4.1 Performance measurings of PI and TSKFNN-AMF controls under healthy condition.

Tracking Errors, rpm	PI Control		TSKFNN-AMF Control	
	Case 1	Case 2	Case 1	Case 2
Maximum	261.12	281.6	71.68	107.52
Average	14.51	15.31	11.06	13.39
Standard Deviation	103.23	146.5	37.71	58.92

Table 4.2 Performance measurings of PI and TSKFNN-AMF controls under faulty condition.

Tracking Errors, rpm	PI Control		TSKFNN-AMF Control	
	Case 3	Case 4	Case 3	Case 4
Maximum	348.16	522.24	245.76	307.2
Average	23.47	32.88	19.06	25.82
Standard Deviation	350.77	357.73	191.74	211.72

Academic Performance

1. F. J. Lin et al., “Hybrid supervisory control using recurrent fuzzy neural network controller for tracking periodic inputs,” ***IEEE Trans. Neural Network***, vol. 12, no. 1, pp. 68-90, 2001.
2. F. J. Lin, P. H. Chou, C. S. Chen, and Y. S. Lin, “DSP-based Cross-Coupled Synchronous Control for Dual Linear Motors via Intelligent Complementary Sliding Mode Control,” ***IEEE Trans. Industrial Electronics***, vol. 59, no. 2, pp. 1061-1073, 2012.
3. F. J. Lin, S. Y. Chen, and M. S. Huang, “Intelligent double integral sliding-mode control for five-degree-of-freedom active magnetic bearing,” ***IET Control Theory Applications***, vol. 5, no. 11, pp. 1287-1303, 2011.
4. F. J. Lin, Y. C. Hung, and M. T. Tsai, “Fault tolerant control for six-phase PMSM drive system via intelligent complementary sliding mode control using TSKFNN-AMF,” ***IEEE Trans. Industrial Electronics***, vol. 60, no. 12, pp. 5747-5762, 2013.

Thank You for Your Attention!